Mouse gingival single-cell transcriptomic atlas: An activated fibroblast subpopulation guides oral barrier immunity in periodontitis

Takeru Kondo [1,2], Annie Gleason [1,3], Hiroko Okawa [1,2], Akishige Hokugo [1,4], Ichiro Nishimura [1]*

[1]Weintraub Center for Reconstructive Biotechnology, UCLA School of Dentistry, Los Angeles, CA 90095, USA

[2]Division of Molecular and Regenerative Prosthodontics, Tohoku University Graduate School of Dentistry, Sendai, Miyagi 980-8575, Japan

[3]UCLA Bruin in Genomics Summer Program,

[4]Regenerative Bioengineering and Repair Laboratory, Division of Plastic and Reconstructive Surgery, Department of Surgery, David Geffen School of Medicine at UCLA, Los Angeles, CA 90095, USA

*Corresponding Author:

Ichiro Nishimura, DDS, DMSc, DMD

Weintraub Center for Reconstructive Biotechnology

UCLA School of Dentistry

Box 951668, CHS B3-087, Los Angeles, CA 90095, USA

Tel: +1 (310) 794-7612, Fax: +1 (310) 825-6345

E-mail: inishimura@dentistry. ucla.edu

Abstract

Chronic cardiovascular and metabolic diseases have been linked with oral inflammation in the tooth-supporting gingiva. Therefore, elucidating the mechanisms underlying development of gingival inflammation may hold critical insight into the pathogenesis of these debilitating non-communicable diseases. Here, we report a unique fibroblast subpopulation activated to guide oral inflammation (AG fibroblasts), identified in a single-cell RNA sequencing-based gingival cell atlas constructed from the mouse ligature-induced periodontitis model. Collagen-XIV-positive AG fibroblasts localized beneath gingival epithelium express chemokine ligands and Toll-like receptor-related molecules upon ligature placement, which were linked to receptors expressed by neutrophils and lymphocytes, including innate lymphoid cells (ILCs). We further identify ILCs as the primary source of proinflammatory interleukin-17 cytokines and show that cervical alveolar bone resorption is absent in Rag2$^{-/-}$γc$^{-/-}$, but not Rag2$^{-/-}$, mice suggesting ILC3s mediate the human periodontitis-like phenotype. We therefore propose AG fibroblasts function as a previously unrecognized surveillant to orchestrate chronic gingival inflammation in periodontitis.

Introduction

The oral mucosa must constantly respond to a diverse array of oral microbes, as well as to dietary and airborne antigens, making it one of the most active barrier tissues in the human body[1, 2]. Consequently, oral barrier immunity acts as a crucial surveillance system, which must defend from pathogenic organisms, while ensuring sustained tolerance of commensal microbes and harmless antigens, without excessive inflammation[3]. Within this system, the junction between the gingiva and the tooth surface represents a weak link, wherein the initiation of localized inflammation often leads to chronic gingivitis and periodontitis. Once this gingival inflammation progresses, adjacent alveolar bone supporting the cervical area of the dentition is subjected to a localized, but often severe, osteoclastic bone resorption, resulting in tooth loss and disruption of the maxillofacial structure[4]. Globally, periodontitis ranks among the most significant contributors to poor health and decreased quality of life, imposing substantial economic and healthcare burdens, particularly in low- and middle-income countries[8]. It is therefore acutely important to elucidate the molecular mechanisms underlying the initiation of gingival inflammation, in order to facilitate the development of effective preventive and therapeutic measures for this debilitating condition.

Critically, periodontitis is not only the most frequent cause of tooth loss in adults[5], it is also associated with a number of severe non-communicable diseases, such as metabolic and cardiovascular diseases. A recent systematic review revealed that type 2 diabetes mellitus patients had significantly worse periodontal status with more tooth loss, and the presence of severe periodontitis increased the incidence of type 2 diabetes mellitus by 53%[6]. Chronic inflammatory conditions are also known to increase the risk of cardiovascular diseases, including valvular heart disease. Recently, a possible association has been recognized between periodontal inflammation—distinct from transient bacteremia due to dental procedures—and

atherosclerotic cardiovascular disease[7]. Although a direct causal relationship between these non-communicative diseases and periodontitis has not been established, it is postulated that periodontitis triggers an inflammatory cascade that begins in oral barrier tissues and subsequently spreads throughout the body. Thus, elucidating the mechanisms underlying periodontitis development may further provide insight on the signaling pathways that induce and sustain systemic inflammation.

Clinical characterization of periodontitis patients and observations made during treatment have not yielded a comprehensive understanding of the mechanisms that promote periodontal disease. Rather, our current model for the pathological framework of periodontitis has been reconstructed from animal models, harvested immune cell analyses, and oral microbial associations[4, 9]. Of particular importance has been the development of a ligature-induced periodontitis model in mice, combined with targeted gene mutations[10]. This model has shown that fully developed periodontal inflammation is closely associated with the abundant recruitment and excessive activation of neutrophils[11] and pathological induction of interleukin (IL)-17–secreting proinflammatory effector $CD4^+$ T helper (Th)17 cells[12]. Based on our current understanding of osteoimmunology, it was hypothesized that these pathological immune cells activate osteoclasts, leading to induction of periodontal alveolar bone resorption[13, 14]. However, the precise cascade of events leading to this pathological outcome has not been fully deciphered.

Investigation of the molecular mechanisms underlying chronic inflammation in immunological disorders is an intense area of research. Prior studies have shown that chemokines are involved in the trafficking and activation of inflammatory cells during both homeostasis and disease-associated inflammation[15]. These small proteins, which typically contain disulfide cysteine–cysteine (CC) and cysteine–X–cysteine (CXC) molecular signatures,

act as ligands for cellular receptors that modulate inflammatory signaling pathways[16]. Such chemokine–receptor networks direct the migration of inflammatory cells, potentially amplifying the resulting tissue damage. However, in addition to immune cells, barrier tissues are also composed of epithelial cells and fibroblastic stromal cells, and increasing evidence suggests that stromal cells are involved in innate immune cell regulation[17, 18, 19, 20]. In particular, we and others have found that oral fibroblasts secrete cytokines and chemokines in response to microbial stimuli or a proinflammatory environment, suggesting a possible mechanism by which they may regulate immune cell function[21, 22]. Therefore, a comprehensive elucidation of chemokine–receptor signaling networks will likely need to include all types of gingival cells.

In the present study, to better understand the pathways contributing to chronic oral inflammation, we determined the gingival single-cell transcriptomic atlas of mice with ligature-induced periodontitis and identified a novel subpopulation of fibroblasts activated to guide chronic inflammation (AG fibroblasts). Our findings suggest that chemokines and ligands derived from AG fibroblasts bind to and activate receptors involved in neutrophil and lymphocyte activation. We further show that *Cd4*$^{-}$ innate lymphoid cells (ILCs) produce proinflammatory IL-17 cytokines in the inflamed gingiva, and provide evidence that type 3 ILCs (ILC3s) are responsible for cervical alveolar bone resorption in mice—a pathological feature consistent with the human periodontitis phenotype. Thus, the results from this study identify the AG fibroblast–neutrophil–ILC3 axis as a previously unrecognized mechanism contributing to pathological inflammation in periodontitis.

Results

Alterations in major cell type proportions during periodontitis development

Periodontal disease was induced in C57BL/6J mice by placing a ligature around the maxillary left second molar[23]; gingival defect developed after Day 3 following ligature placement (**Figure 1A and B**). Three-dimensional (3D) reconstruction of micro-computed tomography (microCT) images (**Figure 1C**) further revealed a reduction in alveolar bone height starting from Day 3, which progressively increased on Day 7 (**Figure 1D—figure supplement 1**). Overall, the observed pattern of periodontal tissue degradation was consistent with that reported in previous studies[24, 25].

Left-side palatal gingiva tissue was harvested from mice on Day 0 (*i.e.*, healthy gingiva without ligature placement) and on Days 1, 4, and 7 after ligature placement, and gingival cells were dissociated for single-cell RNA sequencing (scRNA-seq)[22, 26]. On Days 0 and 1, the major cell types identified included epithelial cells expressing cadherin 1 (*Cdh1*)[27] and type XVII collagen (*Col17a1*)[28], fibroblasts expressing type I collagen (*Col1a1*)[29] and lumican (*Lum*)[30], B cells expressing membrane spanning 4 domains A1 (*Ms4a1*)[31] and cluster of differentiation 79A (*Cd79a*)[32], T cells expressing epsilon subunit of T cell receptor complex (*Cd3e*)[33] and cluster of differentiation 5 (*Cd5*)[34], and myeloid cells expressing lysozyme 2 (*Lyz2)*[35] and integrin subunit alpha M (*Itgam*)[36] (**Figure 1E and F—figure supplement 2**). On Days 4 and 7, an additional endothelial cell fraction expressing selectin P (*Selp*)[37] and selectin E (*Sele*)[38] emerged (**Figure 1E and F—figure supplement 2**), suggesting increased inflammatory neovascularization with the progression of periodontal inflammation. The proportion of B cells was increased on Day 1, and the proportion of myeloid cells increased progressively from Day 4 to 7 (**Figure 1F**). In addition, the proportion of fibroblasts was increased on Day 7 (**Figure 1F**).

Myeloid cell composition and activity during periodontitis development

The infiltration of proinflammatory neutrophils into the gingiva has been extensively characterized in this mouse model of periodontitis[11, 39]. Here, we found that macrophages expressing cluster of differentiation 86 (*Cd86*)[40] and integrin subunit alpha X (*Itgax)*[41] were predominant on Day 0 in the myeloid cell fraction from healthy gingiva (**Figure 2A and B—figure supplement 3**). In contrast, the proportion of neutrophils expressing CXC motif chemokine receptor (*Cxcr2*)[42] and G0/G1 switch gene 2 (*G0s2*)[43] increased after ligature placement and during periodontitis development from Day 1 to 7 (**Figure 2A and B—figure supplement 3**), suggesting continuous neutrophil infiltration into the early and established gingival lesion. Moreover, after ligature placement, gingival neutrophils upregulated the expression of triggering receptor expressed on myeloid cells 1 (*Trem1*), indicating that these cells are activated and participating in the amplification of inflammatory signals[44, 45] (**Figure 2C**). Strikingly, the *Trem1*-expressing activated neutrophils also show upregulation of matrix metalloproteinase 9 (*Mmp9*; **Figure 2C**)—a protein associated with extracellular matrix degeneration within gingival tissue[46]. We further detected expression of tumor necrosis factor alpha (*Tnfa*) and transforming growth factor beta 1 (*Tgfb1*) in both macrophages and neutrophils on Day 0 and after ligature placement (**Figure 2D**). Collectively, these myeloid cell behaviors are consistent with those reported in prior studies on periodontitis development, thus validating our scRNA-seq data.

Myeloid cells are also known to stimulate other immune cells through the expression of CC motif chemokine ligands (CCLs) and CXC motif chemokine ligands (CXCLs), many of which are associated with periodontitis development[47]. Our scRNA-seq analysis revealed that macrophages expressed *Ccl2*, *Ccl9*, Cxcl4, and *Cxcl6*, and neutrophils expressed *Ccl3*, *Ccl4*,

Ccl6, *Cxcl2,* and *Cxcl3* throughout periodontitis development (**Figure 2E and F**). These data suggest that chemokines and cytokines produced by macrophages and neutrophils in inflamed tissue may amplify and polarize the immune response toward chronic gingival inflammation.

Fibroblasts activated to guide leukocyte migration in periodontitis development

We previously identified two distinct subpopulations of gingival fibroblasts, differentiated by expression of type XIV collagen (*Col14a1*)[22], and these were also detected in our current scRNA-seq data from Day 0 to 7 (**Figure 3A**). Gene ontogeny (GO) enrichment analysis of the *Col14a1*-expressing fibroblast subpopulation revealed expression of major gene clusters related to immune regulation, including "Regulation of leukocyte migration" (**Figure 3B**). This immune regulatory phenotype appears to be unique to *Col14a1*-expressing fibroblasts, which are therefore referred to as 'fibroblasts activated to guide leukocyte migration' or AG fibroblasts. The other subpopulation of *Col1a1*-expressing fibroblasts appeared to keep typical fibroblastic features and is thus referred to as KT fibroblasts (**Figure 3C**). An additional fibroblast subpopulation expressing smooth muscle aortic actin 2 (*Acta2*) was detected on Day 7, and these were identified as myofibroblasts[48] (MF) (**Figure 3A**). We found that the proportions of KT and AG fibroblasts were equal on Day 0 and on Days 1 and 4 after ligature placement (**Figure 3E and F**). However, on Day 7, the proportion of AG fibroblasts decreased, and the MF fraction emerged (**Figure 3E and F**).

AG fibroblasts and immune surveillance in periodontitis development

To further characterize AG fibroblasts and their "Regulation of leukocyte migration" phenotype, we analyzed expression of CCL and CXCL chemokines within fibroblast subpopulations in our scRNA-seq dataset[13]. Results show that AG fibroblasts activated expression of *Ccl8, Ccl11,*

Ccl19, Cxcl1, Cxcl11, and *Cxcl12* immediately after ligature placement on Days 1 and 4 (**Figure 4A**). Chemokine expression levels then decreased on Day 7, suggesting that AG fibroblasts might initiate early leukocyte migration into gingival tissue. Given that activation of Toll-like receptors (TLR) is known to increase chemokine expression, we further assessed expression of TLRs in fibroblast subpopulations. We found that AG fibroblasts displayed temporal activation of *Tlr2, Tlr3*, and *Tlr4* expression on Days 1 and 4 (**Figure 4B**). Similarly, the TLR downstream genes *Myd88, Irak1, Map3k7*, and *Rela* were also expressed on Days 1 and 4 (**Figure 4B**). These data suggest that AG fibroblasts may guide the establishment of an early inflammatory environment within the gingiva and thereby promote periodontitis pathogenesis.

To validate the presence of AG fibroblasts, Day 1 gingiva and periodontal tissue histological sections were subjected to immunohistochemistry with antibodies against COL14A1 and CXCL12 (**Figure 4C**). We detected COL14A1- and CXCL12-positive AG fibroblasts localized near gingival epithelial cells in the connective tissue papillae and free gingiva, as well as in the cervical zone of the periodontal ligament (PDL) space (**Figure 4C**). We note that this localization pattern of AG fibroblasts appears to be highly suitable for early immune surveillance during periodontitis pathogenesis.

Role of AG fibroblasts in myeloid cell activation

The interaction between chemokine ligands and their receptors has been extensively studied. Here, to evaluate the interaction between chemokine ligands strongly expressed by AG fibroblasts and chemokine receptors in innate immune cells, we matched AG fibroblast-expressed chemokines to expression of their putative receptors in myeloid cells. Results show that AG fibroblasts may regulate macrophages via the expression *Ccl8* and *Ccl11*, which encode chemokines that can interact with CC chemokine receptors (CCRs) encoded by *Ccr2*

and *Ccr5* in macrophages. Similarly, gene expression signatures suggest that AG fibroblast-mediated neutrophil regulation may occur through CCL8–CCR1, CXCL1–CXCR2, and CXCL12–CXCR4 interactions (**Figure 5A and B**). Notably, all chemokine–receptor pairs are expressed throughout periodontitis development, although expression of factors mediating the interaction between AG fibroblasts and macrophages was decreased on Day 7.

Intercellular communication may occur via other ligand–receptor interactions, which induce downstream target gene expression in recipient cells. Here, we performed NicheNet analysis to identify potential interactions between gingival fibroblasts and myeloid cells, revealing a trend toward increasing ligand–target interactions between fibroblasts and myeloid cells from Day 1 to Day 7 (**Figure 5C and D**). On Day 1, ligand expression was present primarily in AG fibroblasts (**Figure 5E**), whereas on Day 7, MF fibroblasts also exhibited prominent ligand expression (**Figure 5F**). Analysis of target gene expression revealed that both macrophages and neutrophils expressed receptors capable of interacting with AG fibroblast ligands on Day 1 (**Figure 5G**). In contrast, on Day 7, receptor expression was almost exclusively present in neutrophils, suggesting these cells are primarily targeted by MFs and AG fibroblasts at later stages of periodontitis development (**Figure 5H**).

T cells and ILCs in periodontitis development

We next analyzed expression of T cell-related genes in our scRNA-seq dataset and found that the Day 0 healthy gingiva exclusively contained Th cells expressing *Cd4*[49]. However, after ligature placement, cytotoxic T (Tc) cells expressing *Cd8*[49] emerged, and on Day 7, *Cd4*$^{-}$ *Zbtb16*$^{+}$ ILCs and *Cd4*$^{+}$*Foxp3*$^{+}$ regulatory T (Treg) cells[50] were also detected (**Figure 6A and B**). The ILCs expressed *Nfil3*, a basic leucine zipper (bZIP) transcription factor required for ILC development[51] (**Figure 6C**). However, to our surprise, expression of *Rorγ*, *Il17a*, and *Il17f* was

only detected in ILCs (**Figure 6C**), indicating that this gingival subpopulation is predominantly composed of ILC3s.

ILC3s and Th17 cells share similar regulatory functions. However, the role of ILC3s in osteoimmunology has not been fully deciphered. Macrophage-colony stimulating factor (M-CSF), encoded by *Csf1,* and receptor activator of nuclear factor kappa-B ligand (RANKL), encoded by *Tnfsf11,* are known to play critical roles in osteoclast induction. We found that in gingival tissue, AG fibroblasts and neutrophils are the primary cellular sources of *Csf1*; ILC3s also express this gene*,* albeit at lower levels (**Figure 6E**). Expression of *Tnfsf11* was detected in AG fibroblasts and ILC3s (**Figure 6G**). These observations suggest that ILC3s may function as inducers of inflammatory osteoimmune responses, similar to Th17 cells, leading to osteoclastogenesis in periodontitis downstream of AG fibroblast activation.

ILC3s are critical for cervical alveolar bone resorption in the mouse periodontitis model

We next examined the role of ILC3s in periodontitis pathogenesis by measuring ligature-induced gingival defects and alveolar bone resorption in Rag2$^{-/-}$ mice, which lack functional B, Th, and Tc cells, and *Rag2*–IL-2 receptor common gamma (*Il2rg*) double-knockout mice (Rag2$^{-/-}$γc$^{-/-}$), lacking all lymphocytes, including ILCs. After ligature placement, gingival defects developed similarly in wild-type (WT), Rag2$^{-/-}$, and Rag2$^{-/-}$γc$^{-/-}$ mice (**Figure 7A and B**). However, we found that alveolar bone loss was decreased in Rag2$^{-/-}$ mice and nearly eliminated in Rag2$^{-/-}$γc$^{-/-}$ mice (**Figure 7C and D—figure supplement 4A**). MicroCT image analysis further indicated a better perseveration of alveolar bone structure in Rag2$^{-/-}$γc$^{-/-}$ mice, relative to the other groups (**Figure 7C—figure supplement 4B**). Histologically, osteoclastic resorption lacunae were observed on the alveolar bone surface at the cervical PDL and tooth apex PDL zones only in WT mice (**Figure 7E and F**). In addition, we detected a significant decrease in the number of tartrate-

resistant acid phosphatase (TRAP)-positive osteoclasts in the cervical PDL zone of Rag2$^{-/-}$γc$^{-/-}$ mice and in the apical PDL zone of both Rag2$^{-/-}$ and Rag2$^{-/-}$γc$^{-/-}$ mice (**Figure 7G and H**). Collectively, these data suggest that ILC3s, not Th17 cells, are responsible for cervical alveolar bone resorption in the mouse periodontitis model, a pathological phenotype consistent with human disease.

The role of AG fibroblasts and neutrophils in ILC3 development in periodontitis

Based on our present data, we hypothesize that ILC3s within the gingival tissue play a pathological role in alveolar bone resorption in our mouse model. We therefore aimed to identify the cells that promote ILC3 development in mice. Similar to Th17 cells, ILC3 development was shown to be triggered by IL-6 and IL-23a[52, 53]. A survey of our scRNA-seq data identified epithelial cells, fibroblasts, and myeloid cells as the source of *Il6* in gingival tissue (**Figure 8A**). On Days 1 and 4 following ligature placement, AG fibroblasts primarily expressed *Il6,* whereas neutrophils became the predominant source on Day 7. We further found that gingival epithelial cells comprise at least four different subpopulations, plus an additional group displaying an epithelial–mesenchymal transition (EMT) phenotype on Day 7; *Il6* was expressed by several of these epithelial subpopulations, including the EMT subgroup (**Figure 8A—figure supplement 5A–D**). *Il23a* was also detected in AG fibroblasts and myeloid cells (**Figure 8B**), with expression present in all epithelial cell subsets at various points in periodontitis development (**Figure 8B—figure supplement 5D**).

Lastly, we evaluated potential interactions between chemokine ligands expressed by AG fibroblasts and neutrophils and chemokine receptors in innate immune cells. Our data suggest the presence of a chemokine–receptor association between ILC3s and both AG fibroblasts (**Figure 8C**) and neutrophils (**Figure 8D**), although interactions with other innate immune cells

are also possible. NicheNet analysis further identified potential ligand–target gene associations between lymphocytes, including ILC3s, and both fibroblasts (**Figure 8E**) and myeloid cells (**Figure 8F**). Ligand expression was more prominent in AG fibroblasts than in other fibroblast subpopulations (**Figure 8G**) and elevated in neutrophils relative to macrophages (**Figure 8H**). Additionally, target gene expression was detected in ILC3s, although it was not specific to these cells (**Figure 8I, J**). Thus, in total, our data suggest a regulatory role for a newly identified AG fibroblast subpopulation in the gingiva, which appears to orchestrate chronic gingival inflammation, at least in the early stages, and to promote alveolar bone resorption via stimulation of neutrophils and ILC3s.

Discussion

In this study, we used scRNA-seq to generate a gingival cell transcriptomic atlas across the time course of periodontal inflammation development, leading to pathological alveolar bone resorption, in a mouse ligature-induced model of disease. Our results suggest the presence of a unique and previously uncharacterized subpopulation of gingival fibroblasts, referred to as AG fibroblasts, which show upregulated expression of TLRs and chemokines immediately after ligature placement (**Figure 3 and 4**). Previous studies have proposed that TLR-expressing gingival fibroblasts regulate innate immune responses in the oral barrier tissue[54, 55]; however, the precise mechanisms underlying this fibroblast-mediated regulation remained poorly understood. Here, we found that not all gingival fibroblasts acquired an immune-sensing capability, but rather, AG fibroblasts represent a distinct fibroblast subpopulation, capable of upregulating TLRs and potentially responding to microbial and tissue damage signals. Consistent with this possibility, the temporal expression of TLRs was found to be associated with increased expression of CC and CXC chemokine ligands.

The signature gene of AG fibroblasts is *Col14a1*, which encodes a member of the Fibril-Associated Collagen with Interrupted Triple-helices (FACIT) superfamily[56]. To our knowledge, our present findings represent the first observation of COL14A1 in the gingiva (**Figure 4**). However, in a previous study, we detected COL14A1-positive AG fibroblasts immediately under the gingival epithelium and in the cervical region of PDL, making them ideally situated to mediate immune surveillance for oral stimuli and microbial signals[22]. Given the strategic localization within the gingiva and the temporal expression of TLRs and chemokines after ligature placement, we hypothesize that AG fibroblasts play a previously unrecognized role in innate immune regulation during periodontitis development.

Neutrophils are well-established as crucial players in periodontitis progression. One study found that gingival neutrophils in chronic periodontitis patients are longer-lived than those from healthy patients[57]. Moreover, it was shown that dysregulated neutrophils can induce destruction of periodontal connective tissue through the production of toxic molecules, such as reactive oxygen species, leading to initiation of bone resorption[58, 59]. Critically, neutrophil function in periodontitis is dependent on trafficking to the affected gingiva, and accordingly, we found that the proportion of neutrophils increased after ligature placement (**Figure 2**). Neutrophils were previously reported to express a relatively limited number of chemokine receptors, including CXCR2, CXCR4, and CCR1[60, 61]. Consistent with prior studies, we detected expression of these chemokine receptors in gingival neutrophils and linked them to ligands expressed by AG fibroblasts—CXCL1, CXCL12, and CCL8, respectively (**Figure 5).** In addition to chemokines, neutrophils can respond to various chemoattractants that modulate and finetune various cellular behaviors, such as migration direction, adhesion strength, and functional heterogeneity[62]. Here, we observed evidence for substantial intracellular communication between AG fibroblasts and neutrophils through ligand–target gene interactions (**Figure 5**). Although validation of each putative ligand–receptor interaction is beyond the scope of this study, our data suggest that AG fibroblasts may play an important role in neutrophil trafficking in both early and established periodontitis lesions.

A primary pathological consequence of periodontitis is uncontrolled alveolar bone resorption, leading to tooth loss, which is thought to be mediated by osteoimmune pathways involving IL-17–expressing Th17 cells[63]. In contrast, analysis of our scRNA-seq revealed expression of *Rorγ, Il17a*, and *Il17f* not in $CD4^+$ Th cells, but rather, in lymphocytes with ILC characteristics (**Figure 6**). ILCs share phenotypic and functional features with $CD4^+$ T cells, although they lack antigen-specific T cell receptors[51]. In particular, the gingival ILCs detected in

our study strongly expressed *Rorγ*, *Il17a,* and *Il17f,* but not *Tbx21* and *Gata3,* indicating they are ILC3s, which are functionally similar to Th17 cells. Notably, recent clinical studies have reported the presence of ILCs in gingiva from human periodontitis patients[64, 65] and leptin receptor–deficient mice[66]. However, the specific role of these cells in alveolar bone loss had not been previously established.

In the present study, we explored the role of ILC3s in periodontitis-associated bone loss using Rag2$^{-/-}$ and Rag2$^{-/-}$γc$^{-/-}$ mice and observed differential patterns of alveolar bone resorption following ligature placement in these animals. Rag2$^{-/-}$ mutation prevents V(D)J recombination required for generating immunoglobulin and T cell receptors, resulting in the production of functionally immature B and T cells, including Th17 cells. However, ILCs do not undergo genomic receptor rearrangements and, thus, are unaffected by Rag2$^{-/-}$ mutation. In contrast, Rag2$^{-/-}$γc$^{-/-}$ mice have the Rag2$^{-/-}$ mutation in combination with the Il2rg$^{-/-}$ mutation, which disables common γ chain cytokines (γc). Therefore, in addition to non-functional B and T cells, these animals also have defective γc-dependent ILCs. Here, we found that Rag2$^{-/-}$ mice contained a reduced number of osteoclasts in the apical PDL area, indicative of reduced bone resorption in this region, whereas a significant loss of bone resorption was present in both the cervical and apical PDL areas of Rag2$^{-/-}$γc$^{-/-}$ mice (**Figure 7**). Human periodontitis induces alveolar bone at the cervical PDL zone relative to the gingival legion. In contrast, apical alveolar bone resorption is observed in clinical cases of root canal infection (apical periodontitis). Therefore, our findings suggest that ILCs, which are differentially impacted by Rag2$^{-/-}$γc$^{-/-}$ *vs*. Rag2$^{-/-}$ mutation, may be involved in human periodontitis-like alveolar bone resorption near the site of gingival inflammation. It must be noted that Rag2$^{-/-}$ and Rag2$^{-/-}$γc$^{-/-}$ mice developed gingival defects similar to WT mice. However, this observation may be explained by results from our previous study, which suggest that early gingival degradation in the mouse model is

mediated by cathepsin K (CTSK) secreted from gingival fibroblasts[22], rather than by activated lymphocytes.

Differentiation of ILC3s and Th17 cells is mediated by similar environmental cues, with IL-6 and IL-23a playing critical roles in both pathways[67, 68]. Our present scRNA-seq data (**Figure 8**) suggest that AG fibroblasts and neutrophils are the primary cellular sources of *Il6* during the early and later stages, respectively, of periodontitis development. In contrast, *Il23a* was found to be expressed by a variety of cell types, such as AG fibroblasts, myeloid cells, and multiple subsets of epithelial cells, including those with an EMT phenotype[69]. Further, CC and CXC chemokine–receptor associations between ILC3s and both AG fibroblasts and neutrophils appeared to be non-specific. Therefore, our data suggest that rather than a specific trigger, the collective gingival environment, which includes AG fibroblasts, might contribute to ILC3 differentiation.

In conclusion, based on our present findings, we propose that a previously unrecognized AG fibroblast subpopulation in the gingiva can facilitate immune surveillance and participate in the pathological regulation of innate immune cells, such as proinflammatory neutrophils, within oral barrier tissue (**Figure 9**). Moreover, we hypothesize that ILC3s in the inflamed gingiva play a critical role in pathological alveolar bone resorption in the mouse model of periodontitis and, potentially, in human disease. Thus, the newly proposed AG fibroblast–neutrophil–ILC3 axis may hold valuable clues for unraveling the pathological mechanisms underlying periodontitis development. Moreover, these findings also provide a basis for investigation of new preventive and therapeutic strategies to contain oral barrier inflammation and potentially sever the link between periodontitis and debilitating non-communicative metabolic and cardiovascular diseases.

Methods

Animal care

All protocols for animal experiments were reviewed and approved by the University of California Los Angeles (UCLA) Animal Research Committee (ARC# 2003-009) and followed the Public Health Service Policy for the Humane Care and Use of Laboratory Animals and the UCLA Animal Care and Use Training Manual guidelines. C57BL/6J WT, Rag2$^{-/-}$, and Rag2$^{-/-}$γc$^{-/-}$ mice were purchased from the Jackson Laboratory (Bar Harbor, ME, USA). Animals had free access to regular rodent diet and water and were maintained in standard housing conditions with 12-h light/dark cycles in the Division of Laboratory Animal Medicine at UCLA.

Evaluation of gingival defect and alveolar bone resorption in a ligature-induced mouse model of periodontitis

A silk thread was gently tied around the left maxillary second molar of 8- to 12-week-old female WT, Rag2$^{-/-}$, and Rag2$^{-/-}$γc$^{-/-}$ mice under general inhalation anesthesia with isoflurane (Henry Schein, Melville, NY, USA). On Days 1, 3, and 7 after ligature placement, WT mice were randomly chosen and euthanized by 100% CO_2 inhalation. WT mice without ligature placement were used as Day 0 pre-periodontitis control. Rag2$^{-/-}$ and Rag2$^{-/-}$γc$^{-/-}$ mice were euthanized on Day 7. The palatal tissue was digitally photographed, and maxillae were harvested and fixed in 10% buffered formalin (Thermo Fisher Scientific, Waltham, MA, USA). The gingival defect area was measured from digital photographs, using the ImageJ Java-based image-processing program (NIH, Bethesda, MD, USA), and normalized to the circumferential area of the maxillary first molar. Fixed maxillae were subjected to microCT imaging at an energy level of 60 kV and 166 μA, and 3D images were reconstructed from microCT scans (Skyscan 1275: Bruker, Billerica, MA, USA). Alveolar bone loss was assessed at three sites (mesiobuccal cusp,

distobuccal cusp, and distal cusp) of the first molar, two sites (mesiobuccal cusp and distobuccal cusp) of the second molar, and one site (buccal cusp) of the third molar by measuring the distance from the cementoenamel junction (CEJ) to the alveolar bone crest (ABC) on the buccal and palatal side of the alveolar bone. Total bone loss was calculated from the six-site total CEJ–ABC distance. The bone volume/total volume (BV/TV) ratio, bone surface, trabecular number (Tb.N), and trabecular thickness (Tb.Th) in the buccal side of alveolar bone of the second molar were determined using the proprietary analysis program (CTan: Bruker, Billerica, MA, USA). Statistical analysis to assess differences among multiple experimental groups was performed using two-way analysis of variance (ANOVA) with Tukey's multiple-comparison test; $p < 0.05$ was considered to be statistically significant.

Single cell dissociation from mouse maxillary gingiva

On Days 1, 4, and 7 after ligature placement, mice were euthanized by 100% CO_2 inhalation. And maxillary gingival tissues (n = 4 per group) were harvested from freshly isolated mouse maxillae.

Collagenase II treatment: The tissues were cut into 1-mm pieces and placed immediately into digestion buffer, containing 1-mg/ml collagenase II (Life Technologies, Thermo Fisher Scientific, Waltham, MA, USA), 10-units/ml DNase I (Sigma–Aldrich, St. Louis, MO, USA), and 1% bovine serum albumin (BSA; Sigma–Aldrich) in Dulbecco's Modified Eagle Medium (DMEM; Life Technologies). The tissues were incubated in digestion buffer for 20 min at 37 °C on a shaker at 150 rpm and then passed through a 70-µm cell strainer. The collected cells were pelleted at 1,500 rpm for 10 min at 4 °C and resuspended in phosphate-buffered saline (PBS; Life Technologies), supplemented with 0.04% BSA (Cell suspension A).

Trypsin treatment: Immediately following collagenase II treatment, tissues were incubated in 0.25% trypsin (Life Technologies) and 10-units/ml DNase I for 30 min at 37 °C on a 150-rpm shaker. Trypsin was neutralized with fetal bovine serum (Life Technologies), and the tissues were passed through a 70-µm cell strainer and washed with DMEM. The collected cells were then pelleted at 1,500 rpm for 10 min at 4 °C and resuspended in PBS with 0.04% BSA (Cell suspension B). Cell suspension A and Cell suspension B were combined in one tube. An equal number of combined cell suspensions A and B from four animals per group were combined for scRNA-seq analysis (10X Genomics, San Francisco, CA, USA).

Cell clustering and Identification

Cell Ranger was used to align reads, generate feature–barcode matrices, and perform clustering and gene expression analyses on the scRNA-seq data, and the output from this program was analyzed using the R-program Seurat (https://satijalab.org/seurat/). Cells with <2,400 genes detected or >1% mitochondrial gene expression were filtered out as low-quality cells. Individual gene counts for each cell were divided by the total gene counts for that cell and multiplied by a scale factor of 10,000; natural-log transformation was then applied to the counts. The FindVariableFeatures function was used to select 2,000 variable genes with default parameters, and the ScaleData function was used to scale and center the counts in the dataset. Principal component analysis and Uniform Manifold Approximation and Projection dimensional reduction were performed on variably expressed genes. The cluster markers were found using the FindAllMarkers function, and cell types were manually annotated based on the cluster markers. Cell types were assigned based on expression of cell marker genes, and gene expression within different cell types was displayed using dot plots and violin plots.

Histological analysis

Fixed maxillae were decalcified in 10% EDTA (Sigma–Aldrich) for 3 weeks and then embedded in paraffin. Histological cross-sections were stained with hematoxylin and eosin (HE) and evaluated on a light microscope. Adjacent paraffin sections (4 µm) were subjected to a heat-induced epitope retrieval procedure and then immunohistochemically stained with polyclonal antibodies to COL14A1 (#PA5-49916, Thermo Fisher Scientific) and CXCL12 (#PA5-30603, Thermo Fisher Scientific) at a 1:100 dilution, followed by secondary antibody application, diaminobenzidine staining, and methylene blue counterstaining.

Using maxillary cross-sections of WT, Rag2$^{-/-}$, and Rag2$^{-/-}$γc$^{-/-}$ mice, osteoclasts were evaluated by TRAP staining using a commercially available kit (Acid Phosphatase TRAP kit, Sigma–Aldrich), according to the manufacturer's instructions. TRAP-positive cells were counted in the 0.01-mm^2 area. Statistical analysis to assess the differences among multiple experimental groups was performed using two-way ANOVA with Tukey's multiple-comparison test; $p < 0.05$ was considered to be statistically significant.

Functional annotation and pathway enrichment analysis

Annotation and visualization of GO terms were performed by Metascape (http://metascape.org/gp/index.html#/main/step1). The top-100 differentially expressed genes in each population were input and filtered with the term "immune". Filtered genes were then input, and only "biological process" gene sets were retrieved from the GO database.

Ligand–target matrix prediction

NicheNet (v.1.0.0, https://github.com/saeyslab/nichenetr) was used to predict interactions between cell types. In brief, the integrated Seurat object containing each cell subpopulation was

input into the NicheNet Seurat wrapper. Sender cells and receiver cells were determined, and interactions between active ligands expressed by sender cells and target receptors expressed by receiver cells were predicted based on information in signaling and ligand–receptor databases.

Acknowledgements

This study was supported by NIH grants R01DE022550, R44DE025524, and C06RR014529 and by SINTX Technologies.

Author contributions

I.N. conceptualized the project and obtained funding. T.K. and A.H. performed animal studies. H.O. collected microCT data from the animal model. T.K. and A.G. performed scRNA-seq and data analysis. T.K. and I.N. drafted the manuscript. All authors gave final approval and agreed to be accountable for all aspects of the work.

Competing interests

I.N. is a consultant for FUJI FILM Corp and BioVinc LLC and received a research fund from SINTX Technologies, Inc. I.N. and A.H. received a research fund from Maruho Co. Ltd. The other authors declare no competing interests.

Data availability statement

We specify where the data supporting the results of this study can be found and provide hyperlinks to publicly archived datasets analyzed or generated during the study, where applicable. scRNA-seq data are found in NIH Gene Expression Omnibus (GSE228635).

References

1. Abusleme L, *et al.* The subgingival microbiome in health and periodontitis and its relationship with community biomass and inflammation. *ISME J* **7**, 1016-1025 (2013).

2. Belkaid Y, Harrison OJ. Homeostatic Immunity and the Microbiota. *Immunity* **46**, 562-576 (2017).

3. Moutsopoulos NM, Moutsopoulos HM. The oral mucosa: A barrier site participating in tissue-specific and systemic immunity. *Oral Dis* **24**, 22-25 (2018).

4. Lamont RJ, Koo H, Hajishengallis G. The oral microbiota: dynamic communities and host interactions. *Nat Rev Microbiol* **16**, 745-759 (2018).

5. Helal O, Gostemeyer G, Krois J, Fawzy El Sayed K, Graetz C, Schwendicke F. Predictors for tooth loss in periodontitis patients: Systematic review and meta-analysis. *J Clin Periodontol* **46**, 699-712 (2019).

6. Wu CZ, *et al.* Epidemiologic relationship between periodontitis and type 2 diabetes mellitus. *BMC Oral Health* **20**, 204 (2020).

7. Naderi S, Merchant AT. The Association Between Periodontitis and Cardiovascular Disease: an Update. *Curr Atheroscler Rep* **22**, 52 (2020).

8. Peres MA, *et al.* Oral diseases: a global public health challenge. *Lancet* **394**, 249-260 (2019).

9. Hajishengallis G, Chavakis T. Local and systemic mechanisms linking periodontal disease and inflammatory comorbidities. *Nat Rev Immunol* **21**, 426-440 (2021).

10. Lin P, *et al.* Application of Ligature-Induced Periodontitis in Mice to Explore the Molecular Mechanism of Periodontal Disease. *Int J Mol Sci* **22**, (2021).

11. Hajishengallis G. New developments in neutrophil biology and periodontitis. *Periodontol 2000* **82**, 78-92 (2020).

533 12. Hasiakos S, Gwack Y, Kang M, Nishimura I. Calcium Signaling in T Cells and Chronic
534 Inflammatory Disorders of the Oral Cavity. *J Dent Res* **100**, 693-699 (2021).
535
536 13. Cekici A, Kantarci A, Hasturk H, Van Dyke TE. Inflammatory and immune pathways in the
537 pathogenesis of periodontal disease. *Periodontol 2000* **64**, 57-80 (2014).
538
539 14. Ikeuchi T, Moutsopoulos NM. Osteoimmunology in periodontitis: a paradigm for Th17/IL-17
540 inflammatory bone loss. *Bone* **163**, 116500 (2022).
541
542 15. Sokol CL, Luster AD. The chemokine system in innate immunity. *Cold Spring Harb Perspect*
543 *Biol* **7**, (2015).
544
545 16. Hughes CE, Nibbs RJB. A guide to chemokines and their receptors. *FEBS J* **285**, 2944-2971
546 (2018).
547
548 17. Hodzic Z, Schill EM, Bolock AM, Good M. IL-33 and the intestine: The good, the bad, and the
549 inflammatory. *Cytokine* **100**, 1-10 (2017).
550
551 18. Ina K, *et al.* Intestinal fibroblast-derived IL-10 increases survival of mucosal T cells by
552 inhibiting growth factor deprivation- and Fas-mediated apoptosis. *J Immunol* **175**, 2000-2009
553 (2005).
554
555 19. Pinchuk IV, *et al.* PD-1 ligand expression by human colonic myofibroblasts/fibroblasts
556 regulates CD4+ T-cell activity. *Gastroenterology* **135**, 1228-1237, 1237 e1221-1222 (2008).
557
558 20. Cheng HW, *et al.* CCL19-producing fibroblastic stromal cells restrain lung carcinoma growth
559 by promoting local antitumor T-cell responses. *J Allergy Clin Immunol* **142**, 1257-1271 e1254
560 (2018).
561
562 21. Williams DW, *et al.* Human oral mucosa cell atlas reveals a stromal-neutrophil axis
563 regulating tissue immunity. *Cell* **184**, 4090-4104 e4015 (2021).
564
565 22. Kondo T, *et al.* Oral microbial extracellular DNA initiates periodontitis through gingival
566 degradation by fibroblast-derived cathepsin K in mice. *Commun Biol* **5**, 962 (2022).
567

568 23. Abe T, Hajishengallis G. Optimization of the ligature-induced periodontitis model in mice. *J*
569 *Immunol Methods* **394**, 49-54 (2013).
570
571 24. Tamura H, Maekawa T, Hiyoshi T, Terao Y. Analysis of Experimental Ligature-Induced
572 Periodontitis Model in Mice. *Methods Mol Biol* **2210**, 237-250 (2021).
573
574 25. Marchesan J*, et al.* An experimental murine model to study periodontitis. *Nat Protoc* **13**,
575 2247-2267 (2018).
576
577 26. Okawa H*, et al.* Mechanism of bisphosphonate-related osteonecrosis of the jaw (BRONJ)
578 revealed by targeted removal of legacy bisphosphonate from jawbone using competing inert
579 hydroxymethylene diphosphonate. *Elife* **11**, (2022).
580
581 27. Groeger S, Meyle J. Oral Mucosal Epithelial Cells. *Front Immunol* **10**, 208 (2019).
582
583 28. Kamaguchi M*, et al.* High Expression of Collagen XVII Compensates for its Depletion
584 Induced by Pemphigoid IgG in the Oral Mucosa. *J Invest Dermatol* **138**, 1707-1715 (2018).
585
586 29. Takahashi A*, et al.* Autocrine regulation of mesenchymal progenitor cell fates orchestrates
587 tooth eruption. *Proc Natl Acad Sci U S A* **116**, 575-580 (2019).
588
589 30. Lallier TE, Spencer A, Fowler MM. Transcript profiling of periodontal fibroblasts and
590 osteoblasts. *J Periodontol* **76**, 1044-1055 (2005).
591
592 31. Bruno KF, Silva JA, Silva TA, Batista AC, Alencar AH, Estrela C. Characterization of
593 inflammatory cell infiltrate in human dental pulpitis. *Int Endod J* **43**, 1013-1021 (2010).
594
595 32. Sparger EE*, et al.* Investigation of immune cell markers in feline oral squamous cell
596 carcinoma. *Vet Immunol Immunopathol* **202**, 52-62 (2018).
597
598 33. Alcover A, Alarcon B, Di Bartolo V. Cell Biology of T Cell Receptor Expression and Regulation.
599 *Annu Rev Immunol* **36**, 103-125 (2018).
600
601 34. Fujihashi K*, et al.* Immunoregulatory function of CD3+, CD4-, and CD8- T cells. Gamma
602 delta T cell receptor-positive T cells from nude mice abrogate oral tolerance. *J Immunol* **143**,
603 3415-3422 (1989).

604
605 35. Cross M, Mangelsdorf I, Wedel A, Renkawitz R. Mouse lysozyme M gene: isolation,
606 characterization, and expression studies. *Proc Natl Acad Sci U S A* **85**, 6232-6236 (1988).
607
608 36. Okubo M, *et al.* M2-polarized macrophages contribute to neovasculogenesis, leading to
609 relapse of oral cancer following radiation. *Sci Rep* **6**, 27548 (2016).
610
611 37. Gotsch U, Jager U, Dominis M, Vestweber D. Expression of P-selectin on endothelial cells is
612 upregulated by LPS and TNF-alpha in vivo. *Cell Adhes Commun* **2**, 7-14 (1994).
613
614 38. Komatsu T, *et al.* E-selectin mediates Porphyromonas gingivalis adherence to human
615 endothelial cells. *Infect Immun* **80**, 2570-2576 (2012).
616
617 39. Silva LM, Brenchley L, Moutsopoulos NM. Primary immunodeficiencies reveal the essential
618 role of tissue neutrophils in periodontitis. *Immunol Rev* **287**, 226-235 (2019).
619
620 40. Lam RS, *et al.* Macrophage depletion abates Porphyromonas gingivalis-induced alveolar bone
621 resorption in mice. *J Immunol* **193**, 2349-2362 (2014).
622
623 41. Agarbati S, *et al.* Prognostic Relevance of Macrophage Phenotypes in High-grade Oral
624 Tongue Squamous Cell Carcinomas. *Appl Immunohistochem Mol Morphol* **29**, 359-365 (2021).
625
626 42. Hashim A, Alsam A, Payne MA, Aduse-Opoku J, Curtis MA, Joseph S. Loss of Neutrophil
627 Homing to the Periodontal Tissues Modulates the Composition and Disease Potential of the
628 Oral Microbiota. *Infect Immun* **89**, e0030921 (2021).
629
630 43. Zhang F, Zhu YL, Deng WL, Zhu J, Zhang J. Activation of G0S2 is coordinated by
631 recruitment of PML/RARalpha and C/EBPepsilon to its promoter during ATRA-induced APL
632 differentiation. *J Leukoc Biol* **101**, 655-664 (2017).
633
634 44. Bouchon A, Dietrich J, Colonna M. Cutting edge: inflammatory responses can be triggered by
635 TREM-1, a novel receptor expressed on neutrophils and monocytes. *J Immunol* **164**, 4991-
636 4995 (2000).
637

638 45. Dopheide JF, *et al.* Critical limb ischaemia is characterised by an increased production of
639 whole blood reactive oxygen species and expression of TREM-1 on neutrophils.
640 *Atherosclerosis* **229**, 396-403 (2013).
641
642 46. Corotti MV, *et al.* Immunolocalization of matrix metalloproteinases-2 and -9 during apical
643 periodontitis development. *Arch Oral Biol* **54**, 764-771 (2009).
644
645 47. Souto GR, Queiroz CM, Jr., Costa FO, Mesquita RA. Relationship between chemokines and
646 dendritic cells in human chronic periodontitis. *J Periodontol* **85**, 1416-1423 (2014).
647
648 48. Sasaki H, *et al.* Neuronal PAS Domain 2 (Npas2)-Deficient Fibroblasts Accelerate Skin
649 Wound Healing and Dermal Collagen Reconstruction. *Anat Rec (Hoboken)* **303**, 1630-1641
650 (2020).
651
652 49. Mahanonda R, *et al.* Memory T cell subsets in healthy gingiva and periodontitis tissues. *J*
653 *Periodontol* **89**, 1121-1130 (2018).
654
655 50. Wei L, Xu M, Xiong H. An update of knowledge on the regulatory role of Treg cells in apical
656 periodontitis. *Oral Dis* **27**, 1356-1365 (2021).
657
658 51. Eberl G, Colonna M, Di Santo JP, McKenzie AN. Innate lymphoid cells. Innate lymphoid
659 cells: a new paradigm in immunology. *Science* **348**, aaa6566 (2015).
660
661 52. Bielecki P, *et al.* Skin-resident innate lymphoid cells converge on a pathogenic effector state.
662 *Nature* **592**, 128-132 (2021).
663
664 53. Powell N, *et al.* Interleukin 6 Increases Production of Cytokines by Colonic Innate Lymphoid
665 Cells in Mice and Patients With Chronic Intestinal Inflammation. *Gastroenterology* **149**, 456-
666 467 e415 (2015).
667
668 54. Qian SJ, *et al.* Single-Cell RNA Sequencing Identifies New Inflammation-Promoting Cell
669 Subsets in Asian Patients With Chronic Periodontitis. *Front Immunol* **12**, 711337 (2021).
670
671 55. Naruishi K. Biological Roles of Fibroblasts in Periodontal Diseases. *Cells* **11**, (2022).
672

673 56. Agarwal P, *et al.* Collagen XII and XIV, new partners of cartilage oligomeric matrix protein
674 in the skin extracellular matrix suprastructure. *J Biol Chem* **287**, 22549-22559 (2012).
675
676 57. Lakschevitz FS, Aboodi GM, Glogauer M. Oral neutrophil transcriptome changes result in a
677 pro-survival phenotype in periodontal diseases. *PLoS One* **8**, e68983 (2013).
678
679 58. Chapple IL, Matthews JB. The role of reactive oxygen and antioxidant species in periodontal
680 tissue destruction. *Periodontol 2000* **43**, 160-232 (2007).
681
682 59. Ryder MI. Comparison of neutrophil functions in aggressive and chronic periodontitis.
683 *Periodontol 2000* **53**, 124-137 (2010).
684
685 60. Sabroe I, Jones EC, Whyte MK, Dower SK. Regulation of human neutrophil chemokine
686 receptor expression and function by activation of Toll-like receptors 2 and 4. *Immunology* **115**,
687 90-98 (2005).
688
689 61. Huston J, 3rd, Muhm JR. Solitary pulmonary nodules: evaluation with a CT reference
690 phantom. *Radiology* **170**, 653-656 (1989).
691
692 62. Metzemaekers M, Gouwy M, Proost P. Neutrophil chemoattractant receptors in health and
693 disease: double-edged swords. *Cell Mol Immunol* **17**, 433-450 (2020).
694
695 63. Deng J, Lu C, Zhao Q, Chen K, Ma S, Li Z. The Th17/Treg cell balance: crosstalk among the
696 immune system, bone and microbes in periodontitis. *J Periodontal Res*, (2021).
697
698 64. Brown JL, Campbell L, Malcolm J, Adrados Planell A, Butcher JP, Culshaw S. Enrichment of
699 Innate Lymphoid Cell Populations in Gingival Tissue. *J Dent Res* **97**, 1399-1405 (2018).
700
701 65. Dutzan N, Konkel JE, Greenwell-Wild T, Moutsopoulos NM. Characterization of the human
702 immune cell network at the gingival barrier. *Mucosal Immunol* **9**, 1163-1172 (2016).
703
704 66. Wang Q, *et al.* Single-Cell Transcriptomic Atlas of Gingival Mucosa in Type 2 Diabetes. *J*
705 *Dent Res* **101**, 1654-1664 (2022).
706
707 67. Klose CS, *et al.* A T-bet gradient controls the fate and function of CCR6-RORgammat+ innate
708 lymphoid cells. *Nature* **494**, 261-265 (2013).

709
710 68. Sawa S, *et al*. Lineage relationship analysis of RORgammat+ innate lymphoid cells. *Science*
711 **330**, 665-669 (2010).
712
713 69. Wadie KW, Bashir MH, Abbass MMS. Epithelial-mesenchymal transition in gingival tissues
714 from chronic periodontitis patients: A case-control study. *Dent Med Probl* **58**, 311-319 (2021).
715
716
717

Figure Legends

Figure 1. Changes in proportions of major cell types during periodontitis development in mice. (**A**) A ligature (5.0 silk suture) was placed around the maxillary second molar (M2) of wild-type (WT) mice. Representative intra-oral photographs of the maxilla on Day 0, prior to ligature placement (healthy gingiva), and on Days 1, 3, and 7 after ligature placement. (**B**) The gingival defect area was measured and normalized to the circumferential area of the maxillary first molar (M1) (n = 6). Gingival defects appeared on Day 3. (**C**) Representative micro-computed tomography (microCT) images of the maxilla taken from the lateral view. (**D**) Alveolar bone loss was determined from the total distance between the cementoenamel junction (CEJ) and the alveolar bone crest (ABC) of the buccal or palatal bone at six sites in the ligated side (n = 6). Alveolar bone loss was apparent on Day 7. (**E**) Single-cell RNA sequencing (scRNA-seq) *t*-distributed stochastic neighbor embedding (*t*-SNE) projection plots showing the major cell types present within gingival tissue during periodontitis development on Day 0, 1, 4, and 7. Colors indicate cell type, as follows: green, epithelial cells; blue, fibroblasts; pink, endothelial cells; yellow, B cells; red, T cells; and purple, myeloid cells. (**F**) Proportion plots showing the relative amounts of each major cell type on Days 0, 1, 4, and 7. Significance was determined by analysis of variance (ANOVA), with Tukey's multiple-comparison test (**B**, **D**). Data are presented as mean values ± standard deviation (SD); $p < 0.05$ was considered statistically significant.

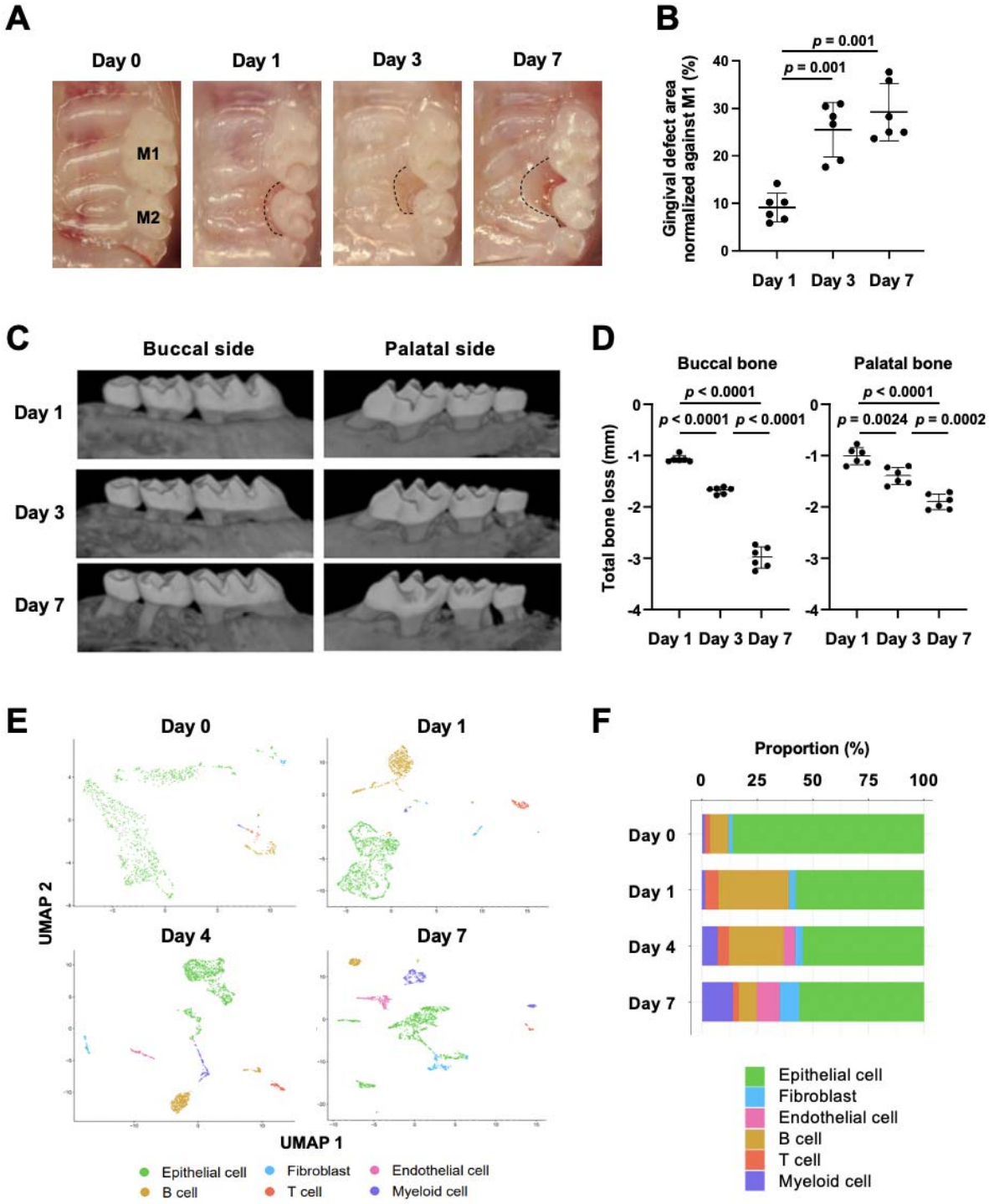
A
Day 0
Day 1
Day 3
Day 7
M1
M2
B
p = 0.001
p = 0.001
Gingival defect area normalized against M1 (%)
40
30
20
10
0
Day 1
Day 3
Day 7
C
Buccal side
Palatal side
Day 1
Day 3
Day 7
D
Buccal bone
Palatal bone
p < 0.0001
p < 0.0001
p < 0.0001
p < 0.0001
p = 0.0024
p = 0.0002
Total bone loss (mm)
0
-1
-2
-3
-4
Day 1
Day 3
Day 7
E
Day 0
Day 1
Day 4
Day 7
UMAP 2
UMAP 1
Epithelial cell
Fibroblast
Endothelial cell
B cell
T cell
Myeloid cell
F
Proportion (%)
0
25
50
75
100
Day 0
Day 1
Day 4
Day 7
Epithelial cell
Fibroblast
Endothelial cell
B cell
T cell
Myeloid cell

736

737

Figure 2. Myeloid cell composition and activity in gingival tissue during in periodontitis development. (**A**) *t*-SNE projection plots showing myeloid cell subpopulations in gingival tissue during periodontitis development on Days 0, 1, 4, and 7. Colors indicate cell type, as follows: green, macrophages and red, neutrophils. (**B**) Proportion plots showing the relative amounts of neutrophils and macrophages on Days 0, 1, 4, and 7. (**C**) Violin plots showing *Trem1* and *Mmp9* expression levels in myeloid cells on Days 0, 1, 4, and 7; both genes are upregulated in neutrophils after ligature placement. (**D**) Violin plots showing *Tgfb1* and *Tnfa* expression in myeloid cells on Days 0, 1, 4, and 7; no obvious induction is observed in response to ligature placement. Dot plots depicting expression levels of the C motif chemokine ligand (CCL) genes *Ccl2*, *Ccl3*, *Ccl4*, *Ccl6*, *Ccl9* (**E**), and the CXC motif chemokine ligand (CXCL) genes *Cxcl2*, *Cxcl3*, *Cxcl4,* and *Cxcl9* (**F**). Chemokine expression in myeloid cells was unrelated to progression of gingival inflammation from Day 1 to 7.

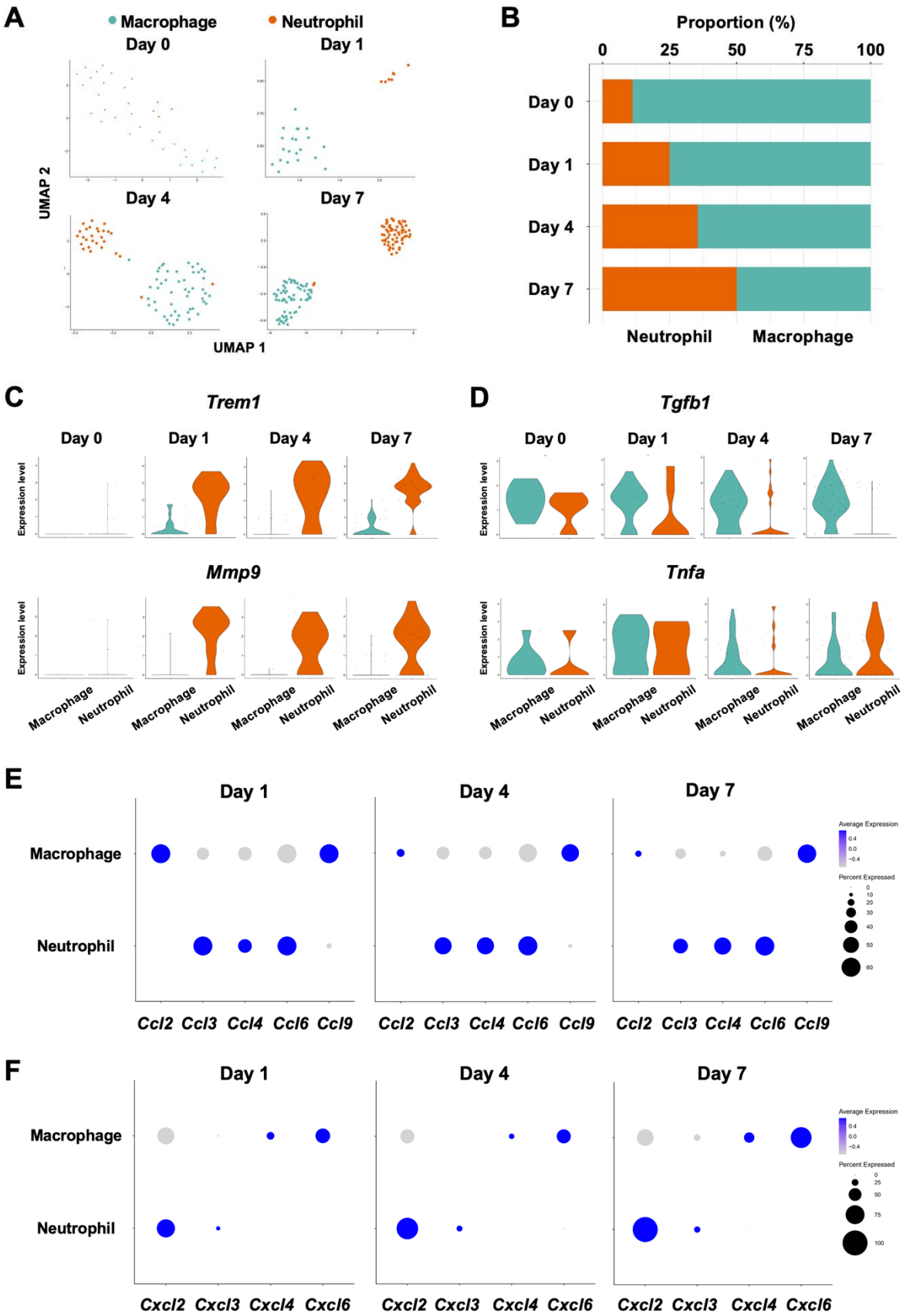
A
Macrophage
Neutrophil
Day 0
Day 1
Day 4
Day 7
UMAP 2
UMAP 1
B
Proportion (%)
0
25
50
75
100
Day 0
Day 1
Day 4
Day 7
Neutrophil
Macrophage
C
Trem1
Day 0
Day 1
Day 4
Day 7
Expression level
Mmp9
Macrophage
Neutrophil
D
Tgfb1
Tnfa
E
Day 1
Day 4
Day 7
Macrophage
Neutrophil
Ccl2 Ccl3 Ccl4 Ccl6 Ccl9
Average Expression
Percent Expressed
F
Cxcl2 Cxcl3 Cxcl4 Cxcl6

750

Figure 3. Fibroblasts activated to guide leukocyte migration (AG fibroblasts) are one of three fibroblast subpopulations in gingival tissue during periodontitis development. (**A**) Violin plots showing gene expression levels of type I collagen (*Col1a1*), type XIV collagen (*Col14a1*), and smooth muscle aortic actin 2 (*Acta2*) in gingival fibroblast subpopulations during periodontitis development. AG, AG fibroblasts; KT, 'keep typical' (KT) fibroblasts; MF, myofibroblasts. Gene ontology (GO) enrichment analysis of the biological functions of AG fibroblasts and KT fibroblasts on Day 0 without ligature placement (**B**) and on Day 1 (**C**) and Day 7 (**D**) after ligature placement. Gene clusters related to immune regulation (red) were identified in AG fibroblasts, and these clusters dominate after ligature placement. (**E**) *t*-SNE projection plots showing fibroblast subpopulations in gingival tissue during periodontitis development. Colors indicate cell type, as follows: blue, KT fibroblasts; red, AG fibroblasts; and yellow, MFs. (**F**) Proportion plots showing the relative amounts of each fibroblast subpopulation on Days 0, 1, 4, and 7.

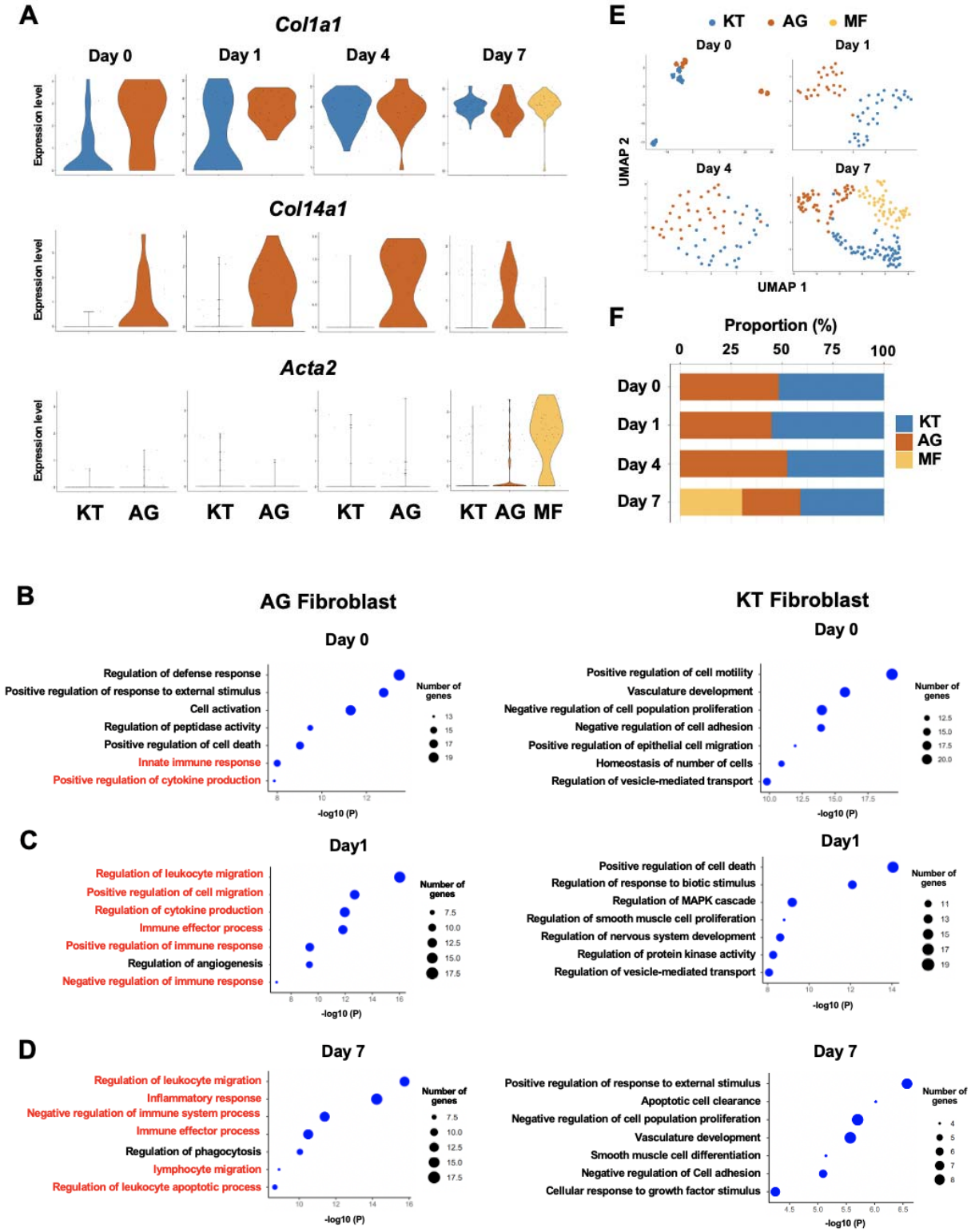
A
Col1a1
Day 0
Day 1
Day 4
Day 7
Expression level
Col14a1
Acta2
KT
AG
MF
E
UMAP 2
UMAP 1
F
Proportion (%)
0
25
50
75
100
B
AG Fibroblast
KT Fibroblast
Regulation of defense response
Positive regulation of response to external stimulus
Cell activation
Regulation of peptidase activity
Positive regulation of cell death
Innate immune response
Positive regulation of cytokine production
Positive regulation of cell motility
Vasculature development
Negative regulation of cell population proliferation
Negative regulation of cell adhesion
Positive regulation of epithelial cell migration
Homeostasis of number of cells
Regulation of vesicle-mediated transport
Number of genes
-log10 (P)
C
Day1
Regulation of leukocyte migration
Positive regulation of cell migration
Regulation of cytokine production
Immune effector process
Positive regulation of immune response
Regulation of angiogenesis
Negative regulation of immune response
Positive regulation of cell death
Regulation of response to biotic stimulus
Regulation of MAPK cascade
Regulation of smooth muscle cell proliferation
Regulation of nervous system development
Regulation of protein kinase activity
Regulation of vesicle-mediated transport
D
Day 7
Regulation of leukocyte migration
Inflammatory response
Negative regulation of immune system process
Immune effector process
Regulation of phagocytosis
lymphocyte migration
Regulation of leukocyte apoptotic process
Positive regulation of response to external stimulus
Apoptotic cell clearance
Negative regulation of cell population proliferation
Vasculature development
Smooth muscle cell differentiation
Negative regulation of Cell adhesion
Cellular response to growth factor stimulus

764
765

Figure 4. AG fibroblasts and immune surveillance in periodontitis development. (**A**) Dot plots depicting expression levels of the CCL genes *Ccl8*, *Ccl11*, *Ccl19*, *Cxcl1*, *Cxcl9*, *Cxcl11*, and *Cxcl12* in gingival fibroblast subpopulations during periodontitis development. (**B**) Dot plots depicting expression levels of the Toll-like receptor and related genes *Tlr2*, *Tlr3*, *Tlr4*, *Myd88*, *Irak1*, *Map3k7*, and *Rela* in gingival fibroblast subpopulations during periodontitis development. Upregulation of chemokines and TLR-related molecules is predominantly observed in the AG fibroblast subpopulation. (**C**) Hematoxylin and eosin (HE) staining and immunohistochemical (IHC) staining for COL14A1 and CXCL12 in periodontal tissue on Day 1; scale bars, 100 µm (HE) and 20 µm, (IHC). Yellow arrows indicate COL14A1- and CXCL12-positive cells in the connective tissue papillae and periodontal ligament (PDL).

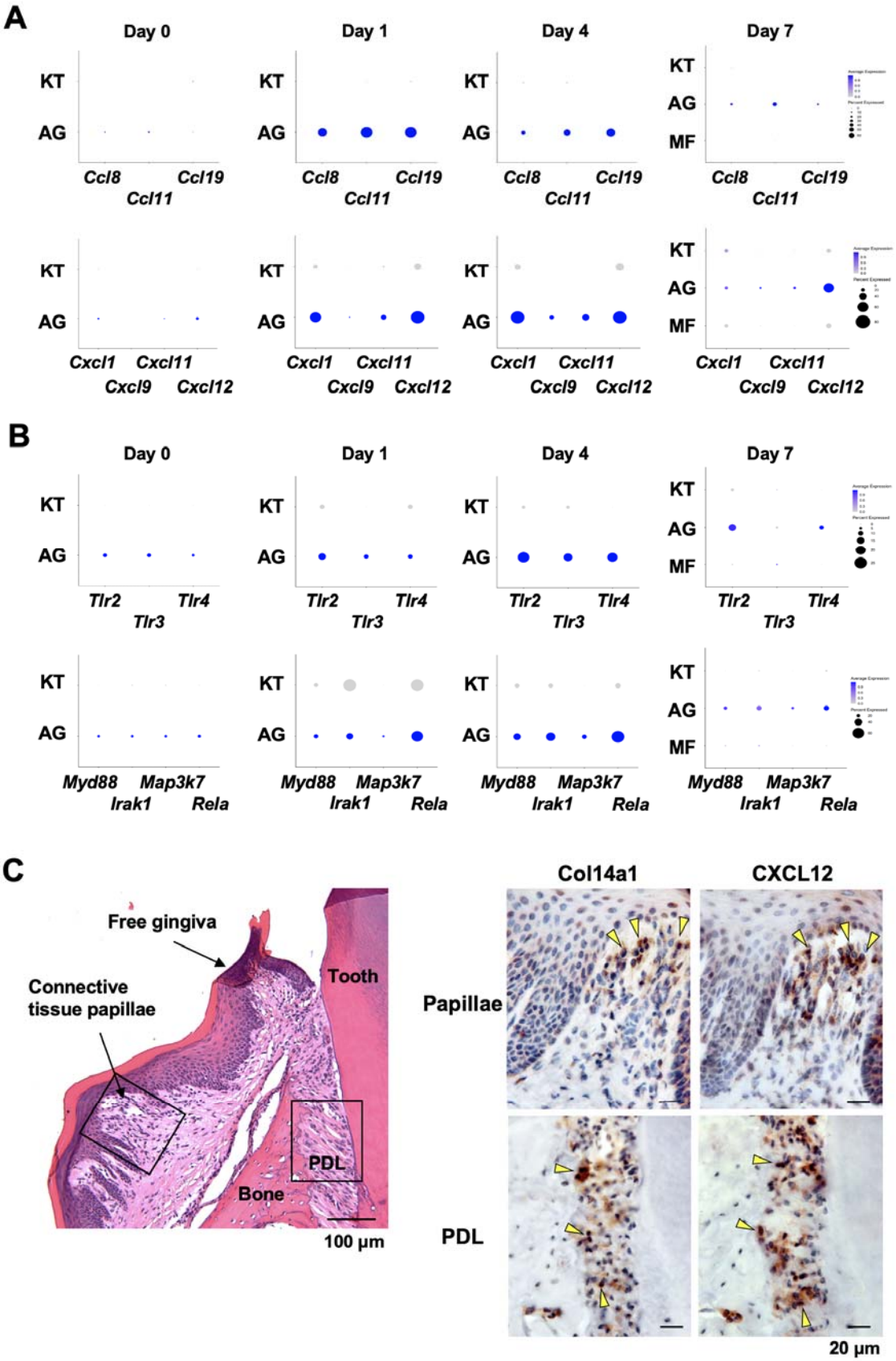
A
Day 0
Day 1
Day 4
Day 7
KT
AG
MF
Ccl8
Ccl19
Ccl11
Cxcl1
Cxcl11
Cxcl9
Cxcl12
B
Tlr2
Tlr4
Tlr3
Myd88
Map3k7
Irak1
Rela
C
Free gingiva
Connective tissue papillae
Tooth
PDL
Bone
100 µm
Col14a1
CXCL12
Papillae
PDL
20 µm

776

Figure 5. Role of AG fibroblasts in myeloid cell activation. Interaction between chemokine ligands expressed by AG fibroblasts and their putative chemokine receptors expressed by myeloid cells during periodontitis development. Dot plots depicting expression levels of the CC chemokine receptor (CCR) and the CXC chemokine receptor (CXCR) genes *Ccr1*, *Ccr2*, *Ccr5*, *Ccr7*, *Cxcr2*, *Cxcr3*, and *Cxcr4* in myeloid cell subpopulations on Day 1 (**A**) and Day 7 (**B**) following ligature placement. NicheNet ligand–target matrix indicating the regulatory potential between active ligands expressed in fibroblasts and target genes expressed in myeloid cells from the p-EMT program on Day 1 (**C**) and Day 7 (**D**). (**E**) Dot plot depicting expression levels of active ligand genes from panel (**C**) in fibroblast subpopulations on Day 1. (**F**) Dot plots depicting expression levels of active ligand genes from panel (**D**) in fibroblast subpopulations on Day 7. (**G**) Dot plot depicting expression levels of target genes from panel (**C**) in myeloid cell subpopulations on Day 1. (**H**) Dot plot depicting expression levels of target genes from panel (**D**) in myeloid cell subpopulations on Day 7. Results suggest a strong intercellular communication network from AG fibroblasts to neutrophils.

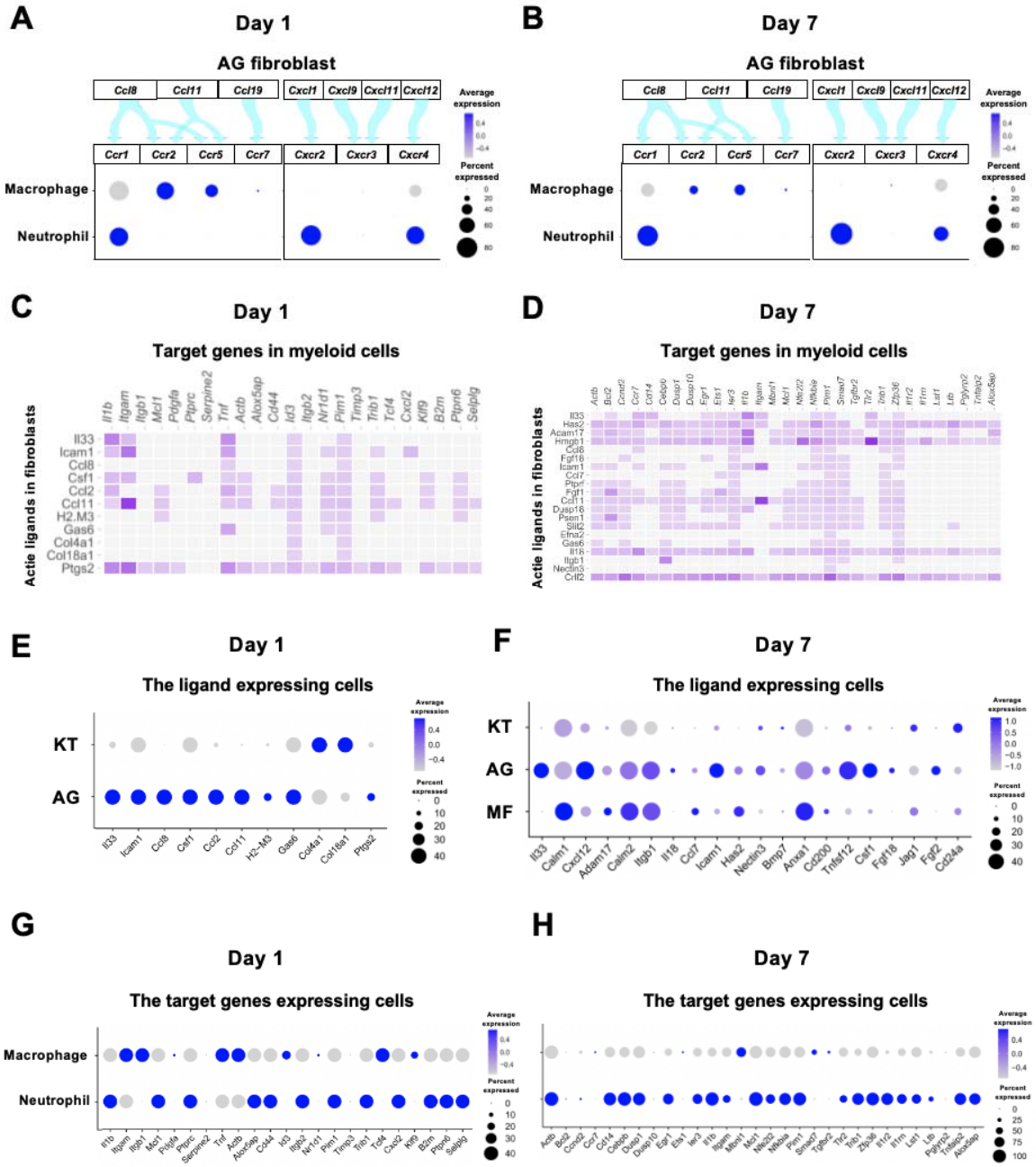
A
Day 1
AG fibroblast
Ccl8
Ccl11
Ccl19
Cxcl1
Cxcl9
Cxcl11
Cxcl12
Ccr1
Ccr2
Ccr5
Ccr7
Cxcr2
Cxcr3
Cxcr4
Macrophage
Neutrophil
Average expression
Percent expressed
B
Day 7
AG fibroblast
C
Day 1
Target genes in myeloid cells
Actie ligands in fibroblasts
D
Day 7
Target genes in myeloid cells
E
Day 1
The ligand expressing cells
KT
AG
F
Day 7
The ligand expressing cells
MF
G
Day 1
The target genes expressing cells
H
Day 7
The target genes expressing cells

Figure 6. T cell subpopulations in periodontitis development. (**A**) Proportion plots showing the relative amounts of T cell subpopulations in gingival tissue during periodontitis development. Treg, T regulatory cells; ILC, innate lymphoid cells; Th, T helper cells; Tc, cytotoxic T cells. (**B**) Violin plots showing expression levels of the T cell marker genes *Cd8* (Tc), *Cd4* (Th), *Zbtb16* (ILC), and *Foxp3* (Treg) on Day 7 following ligature placement. (**C**) Violin plots showing expression levels of *Nfil3*, *Rorγ*, *Il17a*, *Il17f*, *Tbx21*, and *Gata3* on Day 7 following ligature placement. These gene signatures indicate that gingival ILCs primarily comprise type 3 ILCs (ILC3s). (**D**) Violin plots showing expression levels of the macrophage-colony stimulating factor (M-CSF)-encoding gene, *Csf1* (M-CSF), in each major cell type. (**E**) Violin plots showing expression levels of *Csf1* in fibroblast subpopulations, myeloid cell subpopulations, and T cell subpopulations. (**F**) Violin plots showing expression levels of the nuclear factor kappa-B ligand (RANKL)-encoding gene, *Tnfsf11,* in each major cell type. (**G**) Violin plots showing expression levels of *Tnfsf11* in fibroblast subpopulations, myeloid cell subpopulations, and T cell subpopulations.

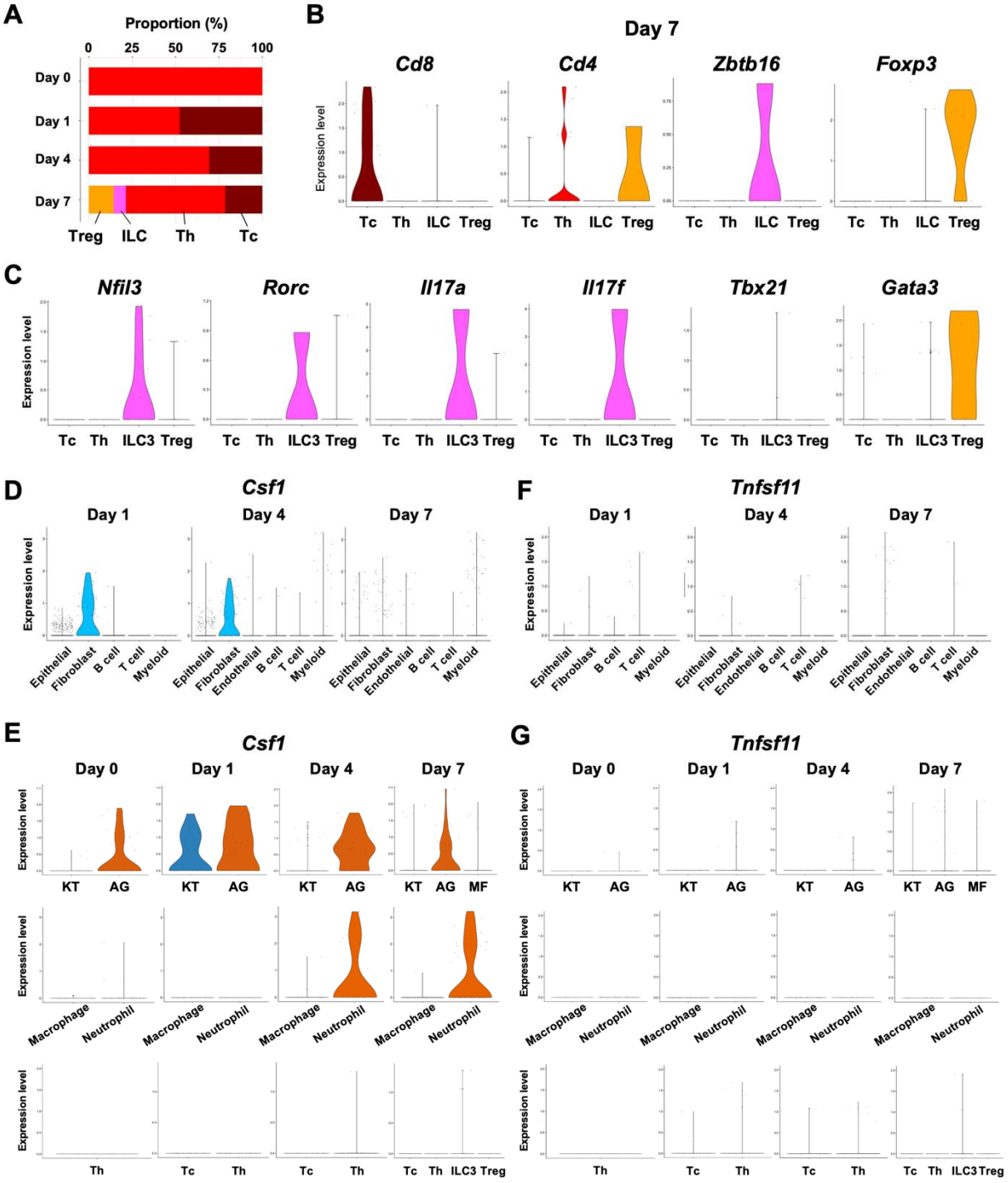
A
Proportion (%)
0 25 50 75 100
Day 0
Day 1
Day 4
Day 7
Treg ILC Th Tc
B
Day 7
Cd8
Cd4
Zbtb16
Foxp3
Expression level
Tc Th ILC Treg
C
Nfil3
Rorc
Il17a
Il17f
Tbx21
Gata3
Expression level
Tc Th ILC3 Treg
D
Csf1
Day 1
Day 4
Day 7
Expression level
Epithelial Fibroblast B cell T cell Myeloid
Epithelial Fibroblast Endothelial B cell T cell Myeloid
F
Tnfsf11
Day 1
Day 4
Day 7
Expression level
Epithelial Fibroblast B cell T cell Myeloid
Epithelial Fibroblast Endothelial B cell T cell Myeloid
E
Csf1
Day 0
Day 1
Day 4
Day 7
Expression level
KT AG
KT AG
KT AG
KT AG MF
Macrophage Neutrophil
Th
Tc Th
Tc Th
Tc Th ILC3 Treg
G
Tnfsf11
Day 0
Day 1
Day 4
Day 7
Expression level
KT AG
KT AG
KT AG
KT AG MF
Macrophage Neutrophil
Th
Tc Th
Tc Th
Tc Th ILC3 Treg

807

808

Figure 7. ILC3s are critical for cervical alveolar bone resorption in the mouse periodontitis model. (**A**) Representative intra-oral photographs of maxilla from WT, Rag2$^{-/-}$, and Rag2$^{-/-}$γc$^{-/-}$ mice taken on Day 7 following ligature placement. (**B**) The gingival defect area was measured and normalized to the circumferential area of M1 (*n* = 5). (**C**) Representative microCT images of the maxilla taken from the lateral view for the ligated side and from the contralateral view for the unligated side. (**D**) Alveolar bone loss was determined from the total distance between the CEJ and the ABC of the buccal bone or palatal bone at six sites in the ligated side (*n* = 6). (**E**) HE staining of the periodontal tissue on Day 7. gCT, gingival connective tissue; Bone, alveolar bone; PDL, periodontal ligament; scale bars, 100 µm. (**F**) Tartrate-resistant acid phosphatase (TRAP) staining of periodontal tissue from WT mice on Day 7; scale bar, 100 µm. Total number of TRAP-positive cells in a 0.01 mm^2-area of the buccal and palatal bone in the cervical PDL site (**G**) and apical PDL site (**H**) (*n* = 6). Significance was determined by ANOVA, with Tukey's multiple-comparison test (**D**, **G**, **H**). Data are presented as mean values ± SD; $p < 0.05$ was considered significant.

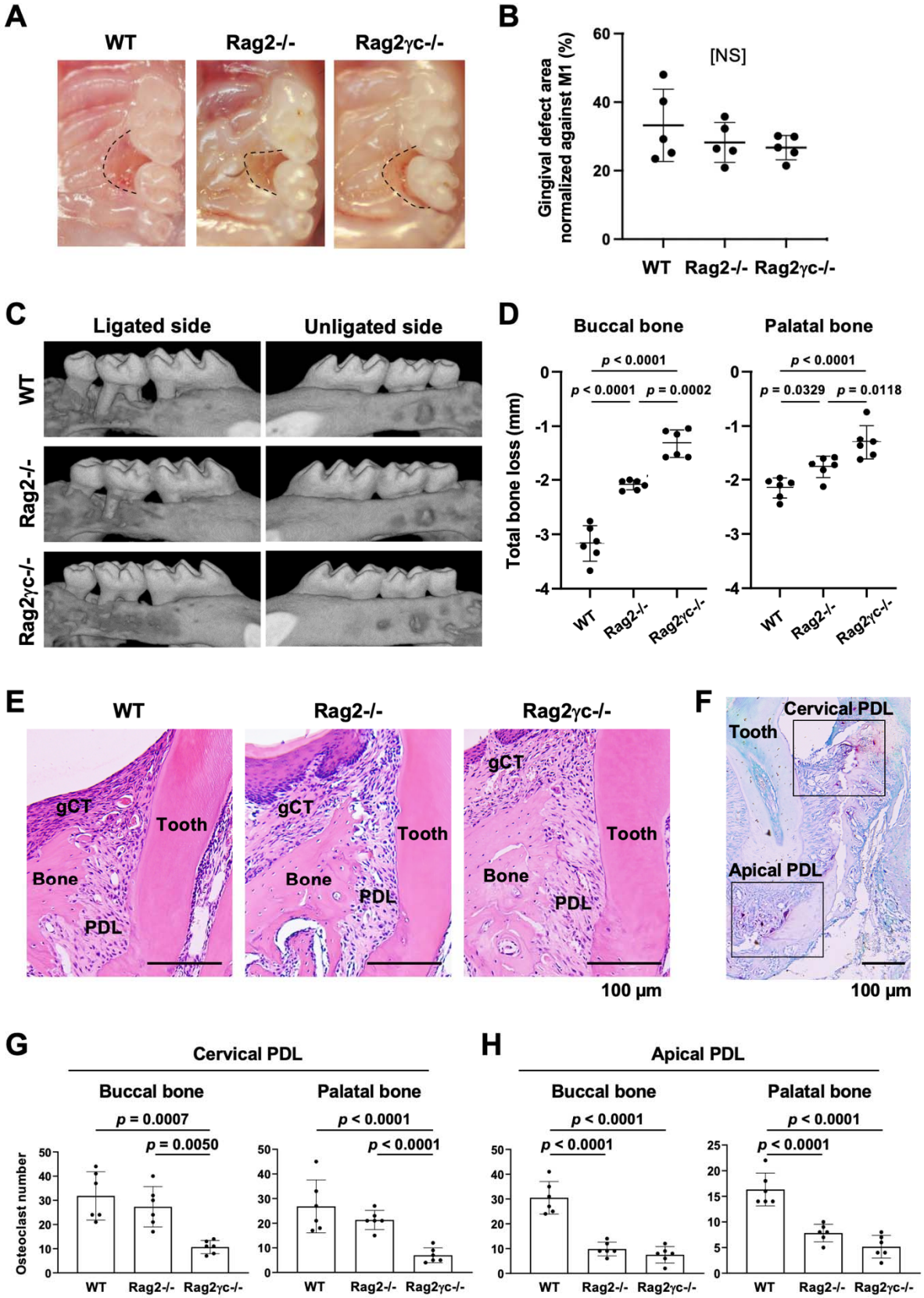
A
WT
Rag2-/-
Rag2γc-/-
B
Gingival defect area normalized against M1 (%)
[NS]
WT
Rag2-/-
Rag2γc-/-
C
Ligated side
Unligated side
WT
Rag2-/-
Rag2γc-/-
D
Buccal bone
Palatal bone
Total bone loss (mm)
p < 0.0001
p < 0.0001
p = 0.0002
p < 0.0001
p = 0.0329
p = 0.0118
E
gCT
Tooth
Bone
PDL
100 µm
F
Cervical PDL
Tooth
Apical PDL
100 µm
G
Cervical PDL
Buccal bone
Palatal bone
Osteoclast number
p = 0.0007
p = 0.0050
p < 0.0001
p < 0.0001
H
Apical PDL
Buccal bone
Palatal bone
p < 0.0001
p < 0.0001
p < 0.0001
p < 0.0001

823

Figure 8. The role of AG fibroblasts and neutrophils in ILC3 development in periodontitis. Violin plots showing expression levels of the genes encoding interleukin (IL)-6 (*Il6)* (**A**) and IL-23 *(Il23a)* (**B**) in each major cell type, fibroblast subpopulations, and myeloid cell subpopulations during periodontitis development. (**C**) Interaction between chemokine ligands strongly expressed by AG fibroblasts and their putative chemokine receptors expressed by T cells, including ILCs. Dot plots depict gene expression levels of *Ccr1*, *Ccr2*, *Ccr5*, *Ccr7*, *Ccr8*, *Cxcr2*, *Cxcr3*, and *Cxcr4* in T cell subpopulations on Day 7 following ligature placement. (**D**) Interaction between chemokine ligands strongly expressed by neutrophils and their putative chemokine receptors expressed by T cells. Dot plots depicting gene expression levels of *Ccr1*, *Ccr4*, and *Ccr5* in T cell subpopulations on Day 7 following ligature placement. (**E**) NicheNet ligand–target matrix denoting the regulatory potential between active ligands in fibroblasts and target genes in T cells from the p-EMT program on Day 7 following ligature placement. (**F**) NicheNet ligand–target matrix denoting the regulatory potential between active ligands in myeloid cells and target genes in T cells from the p-EMT program on Day 7 following ligature placement. (**G**) Dot plot depicting expression levels of active ligand genes from panel (**E**) in fibroblast subpopulations. (**H**) Dot plot depicting expression levels of active ligand genes from panel (**F**) in myeloid cell subpopulations. (**I**) Dot plot depicting expression levels of target genes from pane (**E**) in T cell subpopulations. (**J**) Dot plot depicting expression levels of target genes from panel (**F**) in T cell subpopulations.

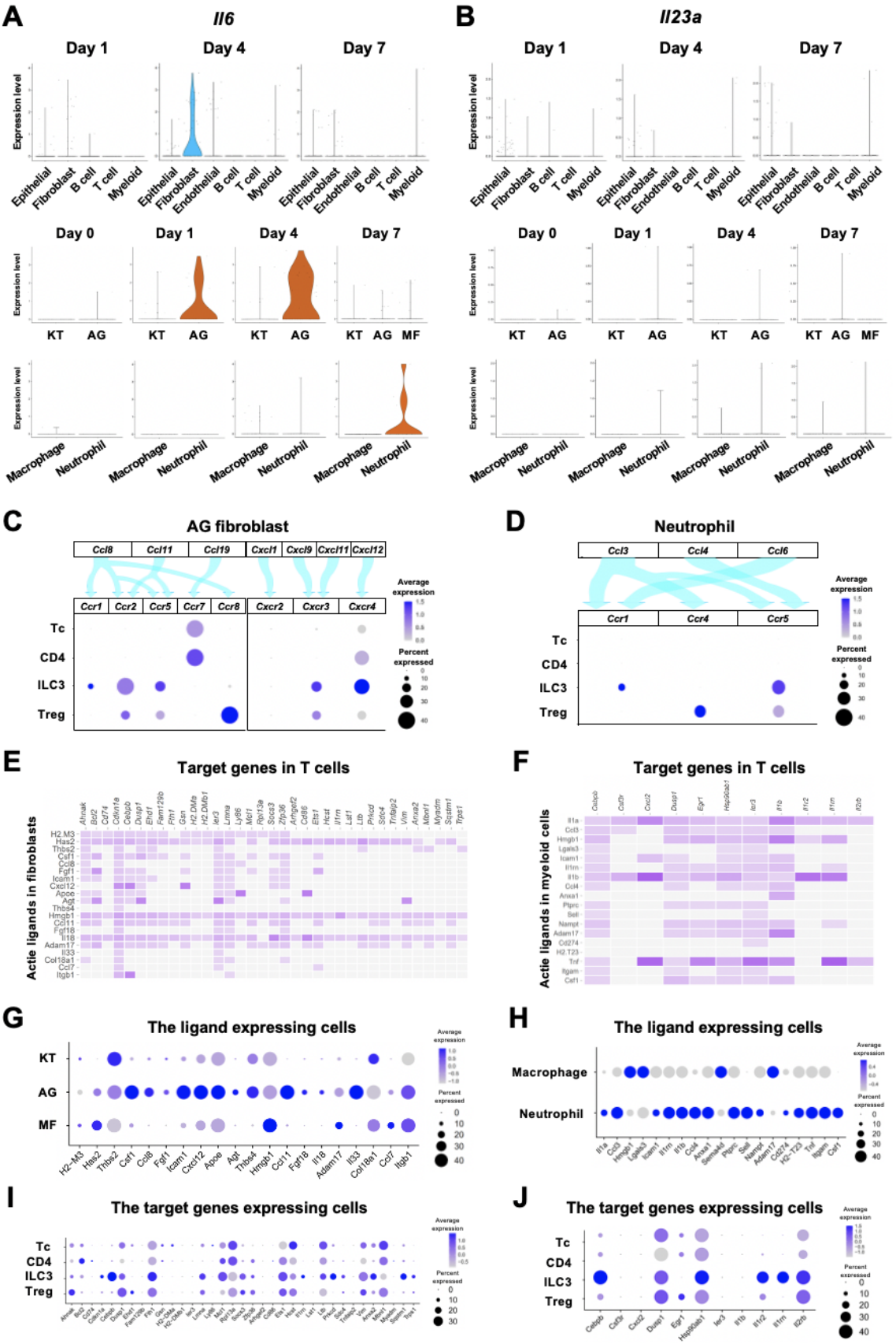
A
Il6
Day 1
Day 4
Day 7
Expression level
Epithelial
Fibroblast
B cell
T cell
Myeloid
Endothelial
Day 0
KT
AG
MF
Macrophage
Neutrophil
B
Il23a
C
AG fibroblast
Ccl8
Ccl11
Ccl19
Cxcl1
Cxcl9
Cxcl11
Cxcl12
Ccr1
Ccr2
Ccr5
Ccr7
Ccr8
Cxcr2
Cxcr3
Cxcr4
Tc
CD4
ILC3
Treg
Average expression
Percent expressed
D
Neutrophil
Ccl3
Ccl4
Ccl6
Ccr1
Ccr4
Ccr5
E
Target genes in T cells
Actie ligands in fibroblasts
F
Target genes in T cells
Actie ligands in myeloid cells
G
The ligand expressing cells
H
The ligand expressing cells
I
The target genes expressing cells
J
The target genes expressing cells

843

Figure 9. Schematic overview of the newly proposed AG fibroblast–neutrophil–ILC3 axis. We propose that periodontal inflammation is initiated by the activation of AG fibroblasts, which secrete chemokines and cytokines that recruit neutrophils to sites of tissue damage. Activated neutrophils and AG fibroblasts, in turn, activate ILC3s, leading to production of proinflammatory IL-17 cytokines. Ultimately, cervical alveolar bone resorption is facilitated by a localized osteoclastogenic environment, induced by activated ILC3s, together with AG fibroblasts, neutrophils, myofibroblasts, and gingival epithelial cells, including those with an epithelial–mesenchymal transition (EMT) phenotype.

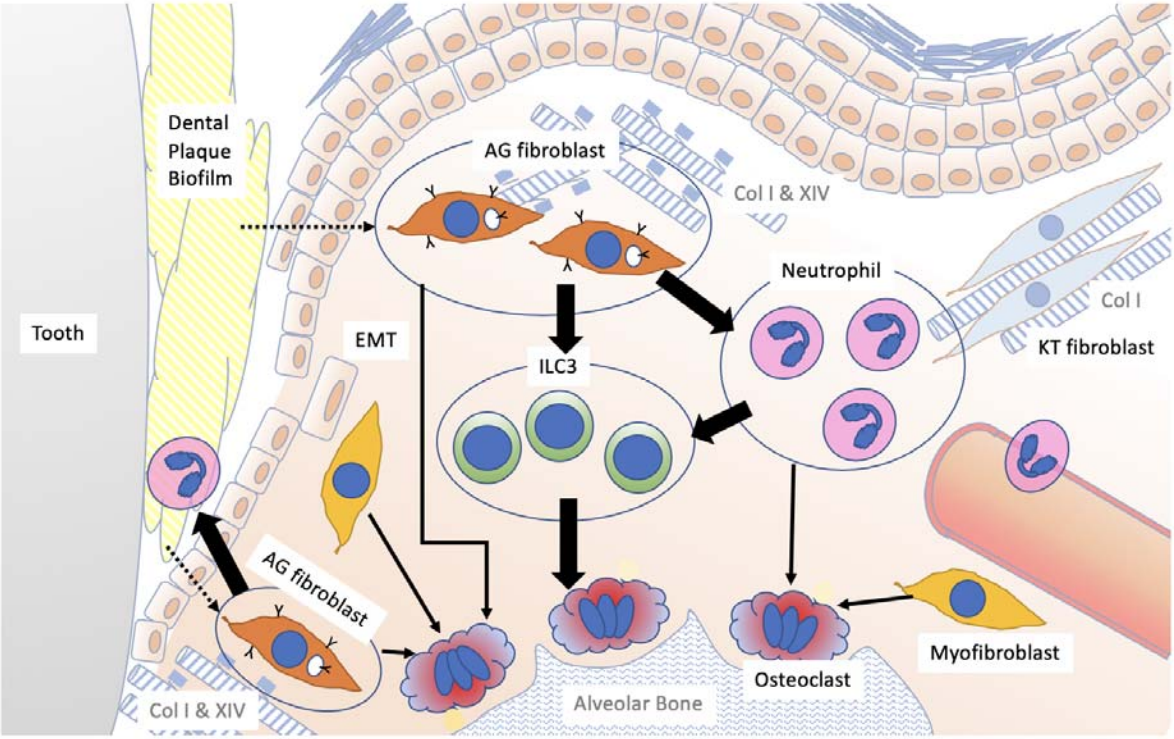

Supplemental Information

Figure supplement 1. Alveolar bone loss in the ligature-induced mouse periodontitis model. Alveolar bone loss was assessed at the mesiobuccal cusp (M1-1), distobuccal cusp (M1-2), and distal cusp (M1-3) of the first molar, the mesiobuccal cusp (M2-1) and distobuccal cusp (M2-2) of the second molar, and the buccal cusp (M3) of the third molar by measuring the distance from the cementoenamel junction (CEJ) to the alveolar bone crest (ABC) on the buccal or palatal side of the alveolar bone (n = 6). Significance was determined by analysis of variance (ANOVA), with Tukey's multiple-comparison test. Data are presented as mean values ± standard deviation (SD); $p < 0.05$ was considered significant.

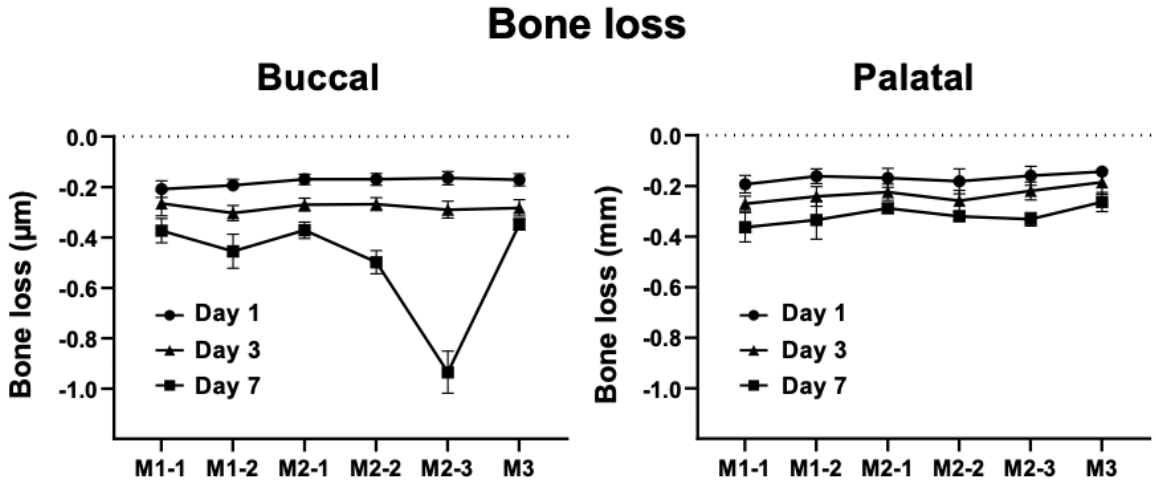

Figure supplement 2. Identification of major cell types in mouse gingival tissue during periodontitis development by single-cell RNA sequencing (scRNA-seq). Violin plots showing expression levels of cell-type marker genes in each major cell type: epithelial cells, cadherin 1 (*Cdh1*) and type XVII collagen (*Col17a1*); fibroblasts, type I collagen (*Col1a1*) and lumican (*Lum*); endothelial cells, selectin P (*Selp*) and selectin E (*Sele*); B cells, membrane spanning 4 domains A1 (*Ms4a1*) and cluster of differentiation 79A (*Cd79a*); T cells, epsilon subunit of T cell receptor complex (*Cd3e*) and cluster of differentiation 5 (*Cd5*); and myeloid cells, lysozyme 2 (*Lyz2*) and integrin subunit alpha M (*Itgam*).

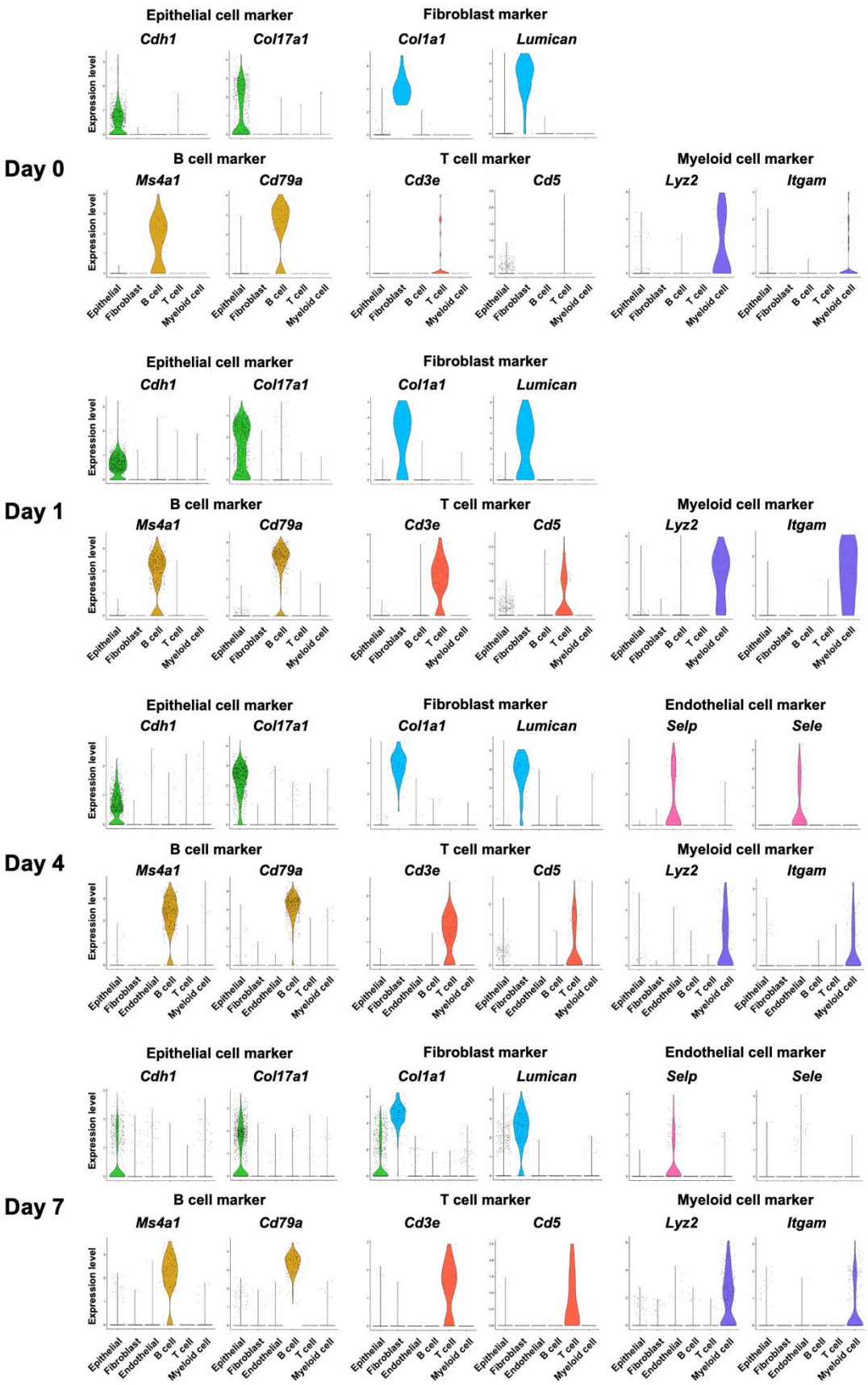
Day 0
Epithelial cell marker
Cdh1
Col17a1
Fibroblast marker
Col1a1
Lumican
B cell marker
Ms4a1
Cd79a
T cell marker
Cd3e
Cd5
Myeloid cell marker
Lyz2
Itgam
Day 1
Epithelial cell marker
Cdh1
Col17a1
Fibroblast marker
Col1a1
Lumican
B cell marker
Ms4a1
Cd79a
T cell marker
Cd3e
Cd5
Myeloid cell marker
Lyz2
Itgam
Day 4
Epithelial cell marker
Cdh1
Col17a1
Fibroblast marker
Col1a1
Lumican
Endothelial cell marker
Selp
Sele
B cell marker
Ms4a1
Cd79a
T cell marker
Cd3e
Cd5
Myeloid cell marker
Lyz2
Itgam
Day 7
Epithelial cell marker
Cdh1
Col17a1
Fibroblast marker
Col1a1
Lumican
Endothelial cell marker
Selp
Sele
B cell marker
Ms4a1
Cd79a
T cell marker
Cd3e
Cd5
Myeloid cell marker
Lyz2
Itgam
Expression level
Epithelial
Fibroblast
Endothelial
B cell
T cell
Myeloid cell

873

Figure supplement 3. Identification of myeloid cell subpopulations in mouse gingival tissue during periodontitis development by scRNA-seq. Violin plots showing expression levels of macrophage and neutrophil marker genes in myeloid cell subpopulations: macrophages, cluster of differentiation 86 (*Cd86*) and integrin subunit alpha X (*Itgax*); and neutrophils, CXC motif chemokine receptor 2 (*Cxcr2*) and G0/G1 switch gene 2 (*G0s2*).

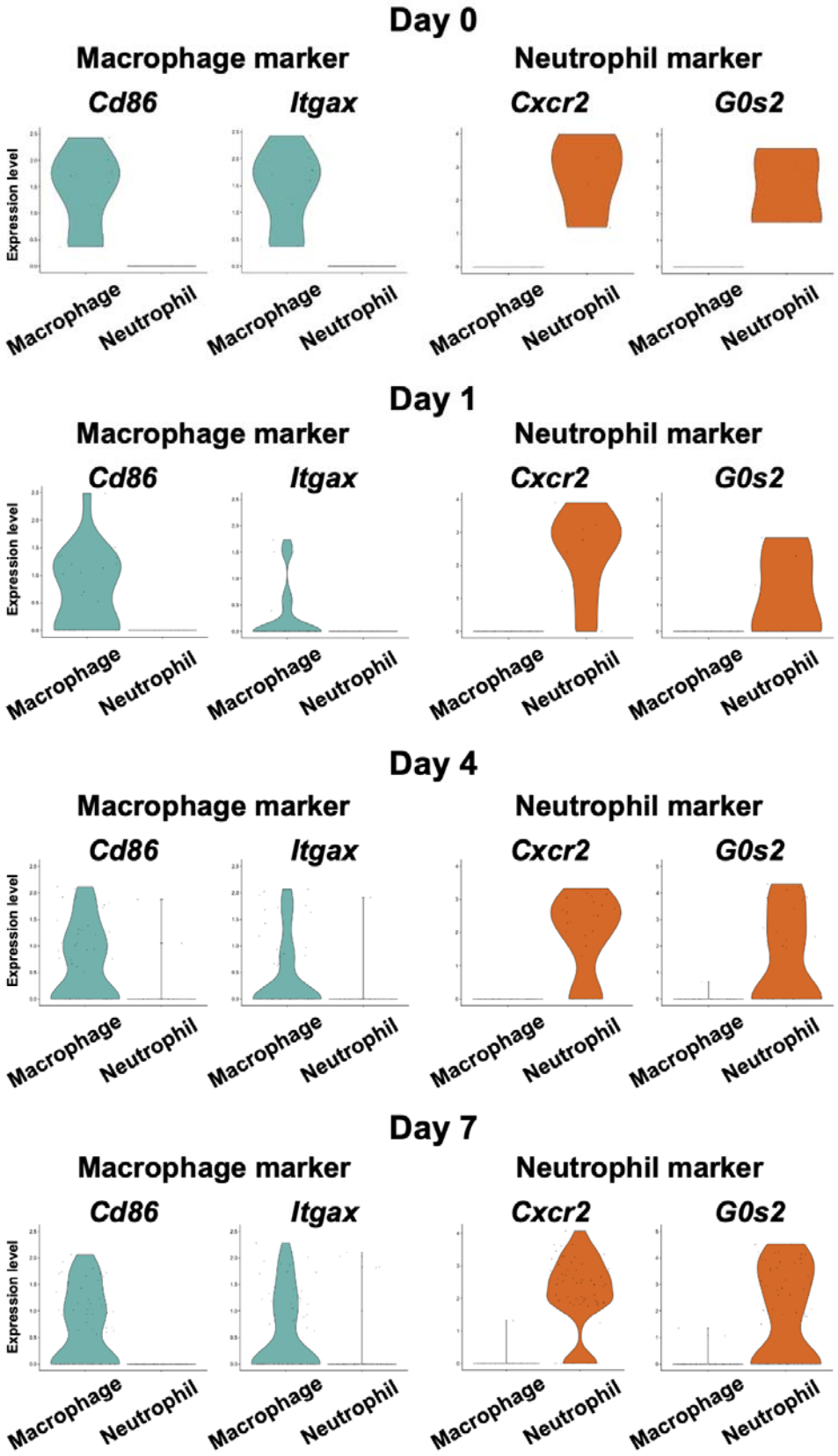
Day 0
Macrophage marker
Neutrophil marker
Cd86
Itgax
Cxcr2
G0s2
Expression level
Macrophage
Neutrophil
Day 1
Day 4
Day 7

879

Figure supplement 4. Effects of innate lymphoid cell (ILC) deletion on alveolar bone loss in the mouse periodontitis model. (**A**) Alveolar bone loss was assessed at six sites by measuring the distance from the CEJ to the ABC on the buccal or palatal side of the alveolar bone of wild-type (WT), Rag2$^{-/-}$, and Rag2$^{-/-}$γc$^{-/-}$ mice on Day 7 following ligature placement (n = 6). (**B**) Bone volume/total volume (BV/TV), bone surface, trabecular number (Tb.N), and trabecular thickness (Tb.Th) in the buccal side of alveolar bone of the second molar were measured on Day 7 (n = 6). Significance was determined by ANOVA, with Tukey's multiple-comparison test. Data are presented as mean values ± SD; $p < 0.05$ was considered significant.

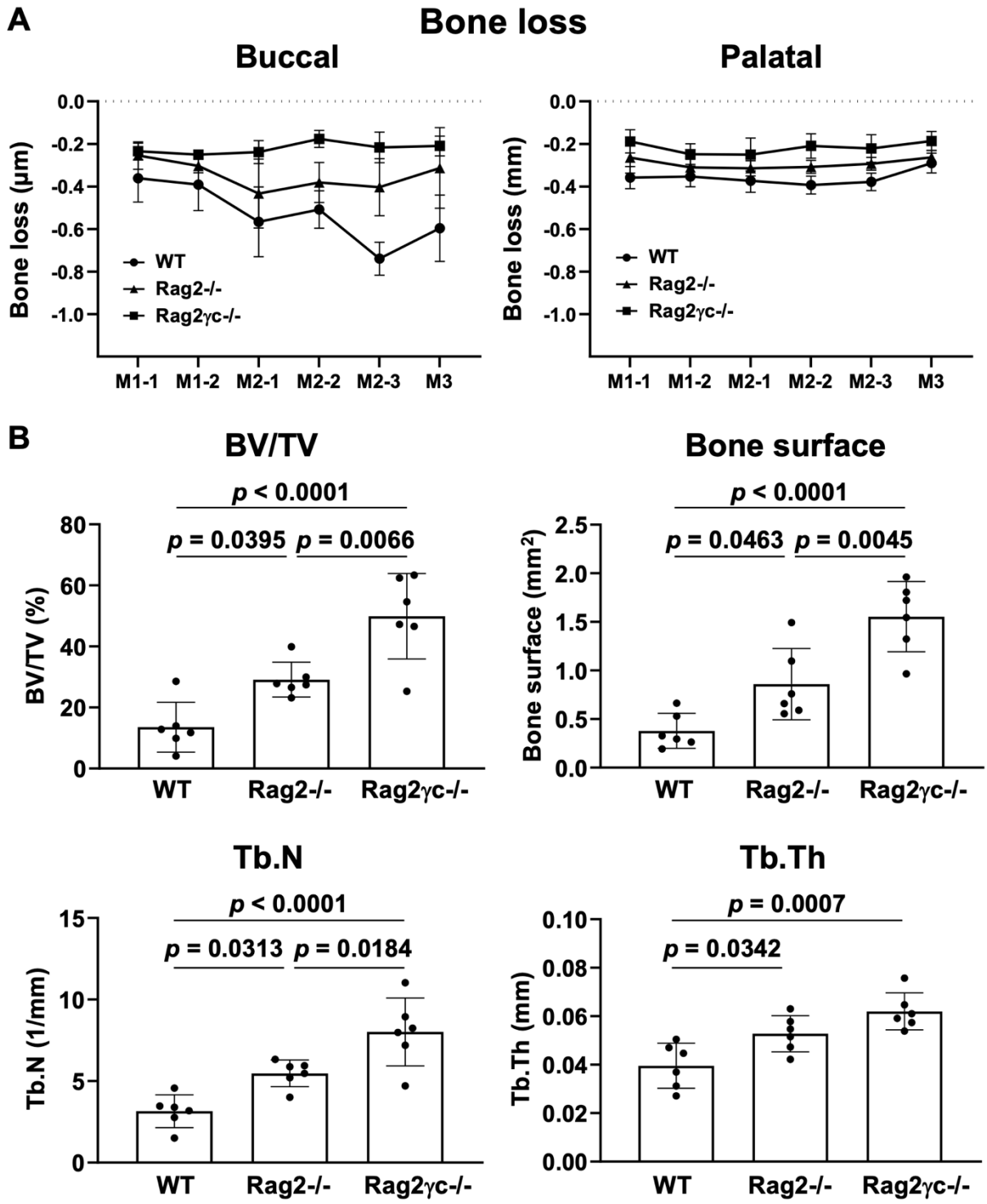
A
Bone loss
Buccal
Palatal
Bone loss (µm)
Bone loss (mm)
0.0
-0.2
-0.4
-0.6
-0.8
-1.0
WT
Rag2-/-
Rag2γc-/-
M1-1
M1-2
M2-1
M2-2
M2-3
M3
B
BV/TV
Bone surface
p < 0.0001
p = 0.0395
p = 0.0066
p = 0.0463
p = 0.0045
BV/TV (%)
Bone surface (mm²)
Tb.N
Tb.Th
p = 0.0313
p = 0.0184
p = 0.0007
p = 0.0342
Tb.N (1/mm)
Tb.Th (mm)

Figure supplement 5. Epithelial cell subpopulations involved in periodontitis development in mice. (**A**) *t*-distributed stochastic neighbor embedding (*t*-SNE) projection plots showing epithelial cell subpopulations in gingival tissue on Days 1, 4, and 7 following ligature placement. Colors indicate cell type, as follows: dark green, epithelial cell population 1 (Epi 1); sea green, epithelial cell population 2 (Epi 2); pale green, epithelial cell population 3 (Epi 3); light green, epithelial cell population 4 (Epi 4); and light blue, epithelial cell population expressing epithelial–mesenchymal transition (EMT) genes. (**B**) Heatmap showing expression of the top-10 differentially expressed genes in Epi 1, Epi 2, Epi 3, Epi4, and EMT. (**C**) Violin plots showing gene expression levels of keratin 5 (*Krt5*), keratin 14 (*Krt14*), cadherin 11 (*Cdh11*), *Col1a1*, tenascin C (*Tnc*), and smooth muscle aortic actin 2 (*Acta2*) in epithelial cell subpopulations. (**D**) Violin plots showing gene expression levels of interleukin 6 (*Il6*) and interleukin 23A (*Il23a*) in epithelial cell subpopulations.

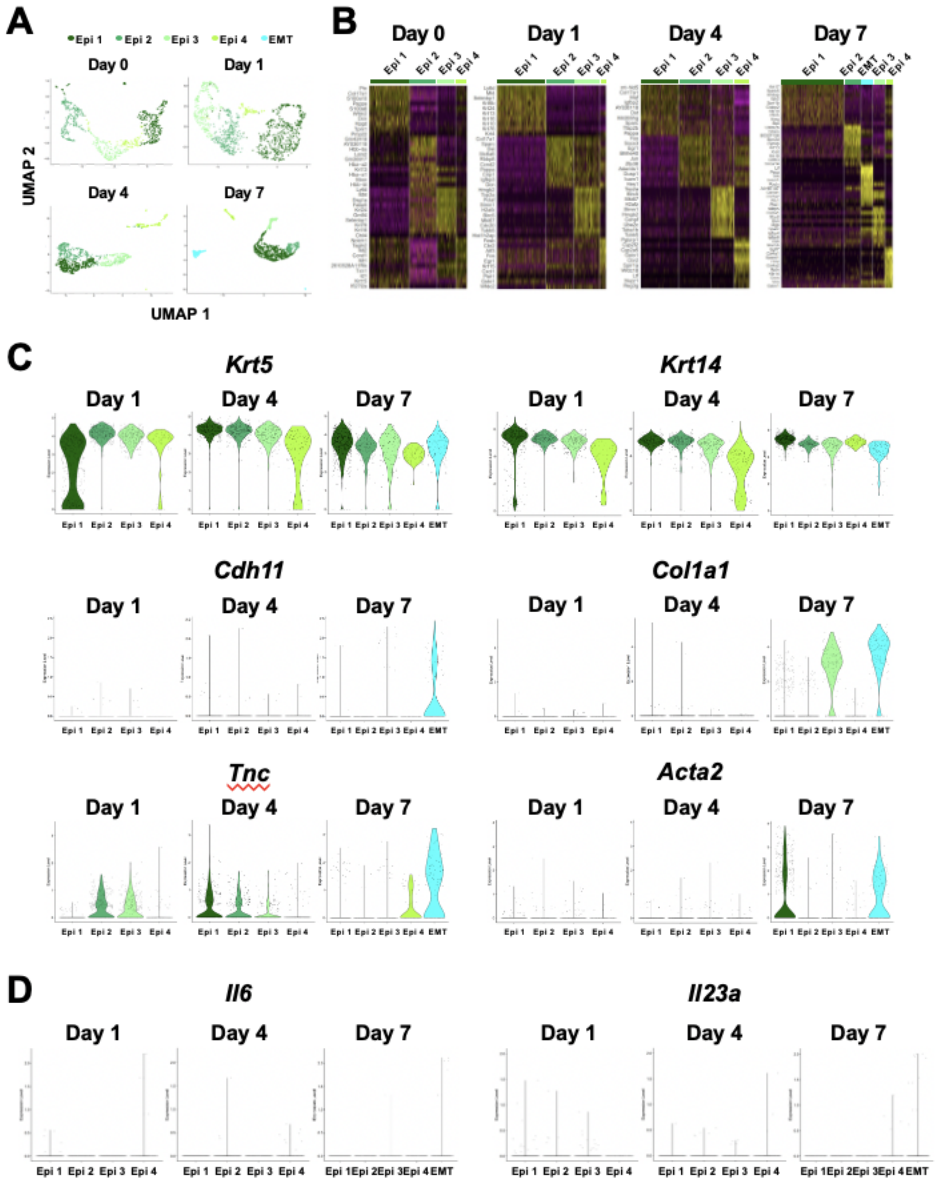

914

915

916